

COUPLED DYNAMICS OF HEAT TRANSFER AND FLUID FLOW IN SHEAR
RHEOMETRY

A Thesis

Presented to

The Graduate Faculty of University of Akron

In Partial Fulfilment

of the Requirements for the Degree

Master of Science in Polymer Engineering

Harini Sridharan

August, 2020

COUPLED DYNAMICS OF HEAT TRANSFER AND FLUID FLOW IN SHEAR
RHEOMETRY

Harini Sridharan

Thesis

Approved:

Accepted:

Advisor
Dr. Ruel McKenzie

Dean of College
Dr. Craig Menzemer

Faculty Reader
Dr. Sadhan Jana

Interim Director, The Graduate School
Dr. Marnie Saunders

Faculty Reader
Dr. Kevin Cavicchi

Date

Department Chair
Dr. Mark Soucek

ABSTRACT

Heat is a ubiquitous phenomenon and its spatial flow has wide reaching impact that spans industry, physiology and even meteorology through examples such as materials processing, thermotaxis and weather patterns. In fluids, spatial heat flow – temperature difference over a characteristic length scale – produces gradients in density and viscosity to generate convective currents which assuredly affects rheological properties and dynamics. The coupled effects between fluid flow and heat flow are phenomenologically explored. To achieve this, a custom-built apparatus capable of introducing, sustaining and measuring heat flux orthogonal to fluid flow was integrated into a stress-controlled rheometer to investigate the impact of steady state temperature gradients on rheological characteristics under steady shear. The novelty of this system is the capacity to independently control temperature of each rheometer plate (i.e. test surface) to establish discreet temperature gradients in the range of -16 K/mm to 30 K/mm, which also gives a window to any potential gravitational effects. Glycerol is used as a model Newtonian fluid to validate the system. Coupled dynamics is scaled by the Brinkman number and Richardson number and is found to have a linear relationship for glycerol. To expand on this knowledge, preliminary data on a more complex (non-Newtonian) system with relevance to heat transfer applications is presented. The rheological and heat flow data was presented using this approach for nanofluids of two weight fractions of Carbon Nanotubes (CNT) in glycerol in order to further understand the implications and opportunities that interrelationships between heat and fluid flow may present in a more complex system.

DEDICATION

Dedicated to the noble profession of teaching and all the cats in the world

ACKNOWLEDGEMENTS

I would like to sincerely thank everybody who has helped me along this incredible journey. I thank Dr. McKenzie for his constant guidance, scientific motivation, support and valuable advice. I would like to thank Dr. Jana for fostering my interest in the subject of Rheology during my first semester in graduate school.

I would like to thank Amma, Appa and Kaavya for their ‘long-distance’ support. This would not have been possible without my roommates, groupmates and essentially family - Vaidehi, Devavrat, Aparna, Sainath, Daria, Albree, Joshua, Alessandro and Brittany (along with their cat Dante) for their fruitful discussions and personal support. I would like to thank my friends back home – Karthikeyan and Loganathan for making me laugh and cry from a thousand miles away.

Last but not the least, I would like to thank my cat Lola who is safely back home and One of a Kind Pet Rescue, Akron for giving me the opportunity to volunteer at their establishment and care for their wonderful dogs and cats.

I would also like to thank my committee for their time and valuable insight to my project.

TABLE OF CONTENTS

LIST OF TABLES.....	viii
LIST OF FIGURES.....	ix
CHAPTER	
I. INTRODUCTION, BACKGROUND AND LITERATURE REVIEWS.....	1
Introduction.....	1
Heat Transfer.....	1
Rheology and Rheometry.....	3
Spatial Temperature Gradients.....	5
Coupled Heat Transfer and Fluid Flow.....	5
Thesis Outline.....	10
II. MATERIALS, METHODS AND DESIGN.....	11
Materials.....	11
Design of Heat Flux Apparatus.....	11
Establishing Temperature Gradient.....	13
Heat Flux Measurement and Analysis.....	14
Rheological Characterisation.....	16
III. APPARATUS VALIDATION.....	18

General Introduction.....	18
Temperature Gradients Established.....	19
Validation Rheological.....	20
Validation – Thermal.....	24
Validation Curves.....	26
Scaling of the experiment.....	27
Discussion.....	29
IV. EXTENSION TO NON-NEWTONIAN FLOW REGIMES.....	31
General Introduction.....	31
Sample Preparation.....	33
Temperature Gradients Established.....	34
Rheological Properties of CNT in glycerol nanofluid.....	35
Thermal Properties of Nanofluid.....	39
Scaling of coupled dynamics.....	40
V CONCLUSION AND FUTURE RESEARCH	
Conclusion.....	42
Future Research.....	43

LIST OF TABLES

Table I Thermal conductivity of select materials at 25°C.....	1
Table II Shear rates tested and corresponding strain and test time.....	17

LIST OF FIGURES

Figure		Page
1.1	Heat Transfer mechanism of conduction in solids and stationary liquids.....2
1.2	Rheometer geometry (a) Parallel plate (b) Cone and Plate (c) Concentric Cylinder.....4
1.3	(a) Thermal Convection currents due to temperature and density gradient in a fluid heated from below (b) Hexagonal convection cells in water studied by Benard above a critical Rayleigh number.....7
1.4	Qualitative comparison of temperature and velocity profile in drag flow (a) without viscous dissipation (b) with viscous dissipation; a non-linear temperature profile develops due to shear heating which subsequently affects the velocity profile.....9
2.1	Schematic of Heat Flux Apparatus system outlining orthogonal superimposition of temperature gradient and shear deformation; T_{UHP} is controlled by the rheometer through convective heating, T_{LHP} is controlled through recirculating chiller.....	...12
2.2	(a) Heat Flux apparatus consisting of UHP and LHP (b) Section view of LHP components (Test Plate, Peltier Plate, Teflon Insulation and Mount) with description of salient features.....	...13
2.3	Sample Performance Curve for glycerol at T_{LHP} 35°C; temperature gradients along the direction of gravity were designated positive and vice-versa.....	...14
2.4	(a) Heat Flux measurement accessories from Fluxteq; Data Acquisition system for measurement of heat flux (Inset) Heat Flux sensor PHFS-01e (b) Thickness of engineered slot in between Test and Peltier Plate for heat flux sensor.....	...15

2.5	Thermal circuit diagram of the heat flux apparatus (a) flux q_1 without fluid sample between UHP and LHP (b) q_2 with fluid sample between UHP and LHP.....	15
3.1	Established temperature gradients for glycerol at constant T_{LHP} : 35°C; temperature gradients were established by keeping T_{LHP} constant and varying T_{UHP}	19
3.2	Viscosity of glycerol in ETC at isothermal conditions across shear rates ranging from $1s^{-1}$ to $100s^{-1}$	20
3.3	$\ln\mu$ vs. $1/T$ for glycerol tested at $1s^{-1}$, $10s^{-1}$ and $100s^{-1}$ (Inset) Fit parameters: A, B.....	21
3.4	Viscosity vs. Temperature gradients at T_{LHP} 35°C, 40°C and 45°C; comparison between analytical model (dotted line) and experimental results (discrete points).....	23
3.5	Viscosity values at isothermal conditions measured in the ETC (dashed line) and Heat Flux Apparatus (Discrete points) at 35°C, 40°C and 45°C.....	24
3.6	Comparison between values reported in literature (dotted line) and experimental values (discrete points) at T_{LHP} 35°C (a) Thermal conductivity of glycerol vs. shear rate (b) Heat flux vs. shear rate.....	25
3.7	Experimental Brinkman number vs γ^2 of select temperature gradients at T_{LHP} 35°C; the experimental Br exhibits an exponent of 1 with γ^2 which is represented by the right triangle.....	26
3.8	Experimental Brinkman number vs. temperature gradient of tested shear rates at T_{LHP} 35°C (only positive gradients shown to enable logarithmic representation); the experimental Br exhibits an exponent of -1 with temperature gradient which is represented by the right triangle.....	27
3.9	Scaled transport dynamics of coupled heat and fluid flow (Br vs. Ri) at T_{LHP} : 35°C, 40°C and 45°C; the experimental data measured at all TLHP at several temperature gradients and lower to intermediate shear rates collapse on a single curve	

	which is fit to a power curve.....	...28
4.1	(a) Structure of Single Wall Carbon Nanotube (b) SEM micrograph of Single Wall Carbon nanotube.....	...31
4.2	Setup for ultrasonication CNT nanofluid; the glass vial containing the nanofluid was suspended in an ice bath to control temperature rise during ultrasonication.....	...34
4.3	Established temperature gradients at T_{LHP} 35°C (a) N0.5 (b) N1.....	...35
4.4	Viscosity of nanofluids in ETC at isothermal conditions across tested shear rates 1 s ⁻¹ to 10 s ⁻¹ (Inset) $\ln\mu$ vs. 1/T at tested shear rates (a) N0.5 (b) N1.....	...36
4.5	Fit parameters of N0.5 and N1 at tested shear rates (a) A (primary y axis) (b) B (secondary y axis); both parameters A and B exhibit shear rate dependence which is fit to a power curve.....	...37
4.6	Model viscosity vs. temperature gradient of N0.5 (discrete points) and N1 (dashed line).....	...37
4.7	Viscosity vs. temperature gradient – analytical model (dashed lines) and experimental (discrete points) values (a) N0.5 (b) N1.....	...39
4.8	Experimental values at T_{LHP} 35C (a) Thermal conductivity vs. shear rate (b) Heat flux vs. shear rate; N0.5 (Hollow points) and N1 (Filled points).....	...40
4.9	Scaled transport dynamics of coupled heat and fluid flow of N0.5 and N1 at T_{LHP} : 35°C, 40°C and 45°C – Br. vs. Ri.....	...41

NOMENCLATURE

<u>Parameter</u>	<u>Unit in SI</u>	<u>Symbol</u>
Heat Flux	W/m^2	q
Temperature	K	T
Gap between surface	m	L
Thermal Conductivity	W/mK	k
Shear Stress	N/m^2	τ
Shear Rate	1/s	$\dot{\gamma}$
Shear	-	γ
Shear Modulus	N/m^2	G
Viscosity	Pa.s	μ
Rotational Velocity	Radian/s	Ω
Radius of Plate	m	R
Radial coordinate	-	r
Rotational Coordinate	-	θ
Vertical Coordinate	-	z
Velocity	m/s	v
Viscous Dissipation	W/m^3	ϕ
Acceleration due to gravity	m/s^2	g
Thermal Expansion Coefficient	1/K	β
Specific Heat Capacity	J/kgK	C_p
Density	kg/m^3	ρ

Sensitivity of Heat Flux sensor	$\mu\text{V}/(\text{W}/\text{m}^2)$	Se
Thermal Resistance of air	K/W	R _a
Thermal Resistance of sensor	K/W	R _{sensor}
Thermal Resistance of Fluid	K/W	R _f
Brinkman Number	-	Br
Richardson Number	-	Ri

CHAPTER I

INTRODUCTION, BACKGROUND AND LITERATURE REVIEW

1.1 Introduction

Heat and its flow along a spatial temperature gradient can be observed in diverse systems in nature that span meteorology¹, physiology² and industrial operations³. The flow of heat is a ubiquitous phenomenon. Processes that occur on a microscopic scale such as locomotion of sperm cells² to macroscopic effects such as climate patterns and rainfall are affected by heat flow. Studying heat and its transfer has led to various leaps in technology and given birth to major technological advancements that harness the potential of thermal energy; equipment such as heat exchangers, boilers, and solar collectors are designed based on heat transfer analysis⁴.

The coupled dynamics of heat transfer and fluid flow can be studied by individually understanding the fundamentals of both the transport dynamics. A succinct summary of heat transfer and rheology are elucidated in the subsequent sections.

1.2 Heat Transfer

The flow of heat is defined by heat flux (q) which is the flow of thermal energy per unit area per unit time. Heat flux is directly proportional to the driving force i.e. temperature difference and inversely proportional to the length of the heat transfer path⁴. Heat is transported through matter by various modes – conduction, convection and radiation. Figure 1.1 is a schematic depicting the conduction mode of heat transfer.

Conduction involves molecular energy transfer in solids and stationary liquids according to Fourier's law of conduction (Equation 1).

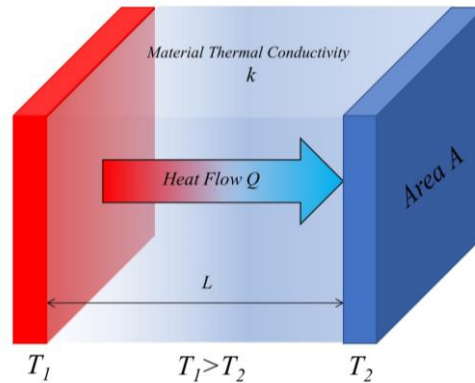


Figure 1.1 Heat Transfer mechanism of conduction in solids and stationary liquids

$$q = k \frac{\Delta T}{L} \quad (1)$$

Thermal conductivity (k) is a material property; it is a function of the overall temperature and pressure of the system. The thermal conductivities of select materials are tabulated in Table 1⁵.

Material	Thermal Conductivity (W/mK)
Air	0.026
Teflon	0.25
Glycerol	0.28
Water	0.6
Stainless Steel	14.4
Aluminium	205
Carbon Nanotube (CNT)	3000

Table 1 Thermal conductivity of common materials used for heat transfer⁵; T = 25°C

Other modes of heat transfer include convection and radiation. Convection is a result of conduction and heat transported through the bulk motion of a fluid at non-uniform temperature whereas radiation occurs through energy emission

(electromagnetic waves). Unlike conduction and convection, radiation can occur even if there is no intervening medium.

1.3 Rheology and Rheometry

Rheology investigates the relationship between force and deformation in a material, both solid and liquid⁶. Materials can be classified based on their response to deformation – purely elastic materials such as metals develop stress that is directly proportional to the strain applied on them whereas purely viscous materials such as water and honey resist deformation and develop stress that is directly proportional to strain rate. Viscoelastic materials, whose behaviour is covered within the scope of rheology, exhibit both viscous and elastic characteristics *e.g.* mayonnaise, elastomers etc.

Materials are studied by drawing fundamental relationships between force and deformation, known as constitutive relations. The simplest constitutive relationship for elastic materials is known as Hooke's law (Equation 2a). Viscous materials can be understood through Newton's law of viscosity (Equation 2b) in which the shear stress (τ) is proportional to the shear rate ($\dot{\gamma}$) and the viscosity of the fluid (μ) does not change with shear rate. Fluids which follow this relationship are known as Newtonian liquids such as water, glycerol etc. Other materials such as silicones, silly putty and paint, whose viscosity is a function of shear rate, are known as non-Newtonian materials. Several constitutive relations such as Power law, Cross and Carreau-Yasuda model were developed to describe the flow of generalised Newtonian fluids⁶.

$$\tau = G\gamma \quad (2a)$$

$$\tau = \mu\dot{\gamma} \quad (2b)$$

The theoretical predictions derived from constitutive relations and mathematical models are compared with experimental data which are collected using different rheological equipment such as parallel plate rheometer, cone and plate rheometer, concentric cylinder rheometer (Figure 1.2 a, b and c respectively) to name a few⁶. The experimental characterisation of the rheological properties of a fluid is called rheometry. Rheometers can be classified according to different parameters that include type of deformation and homogeneity of strain. Rheometers can apply different types of deformation such as shear which is seen in torsional rheometers and elongation in capillary breakup.

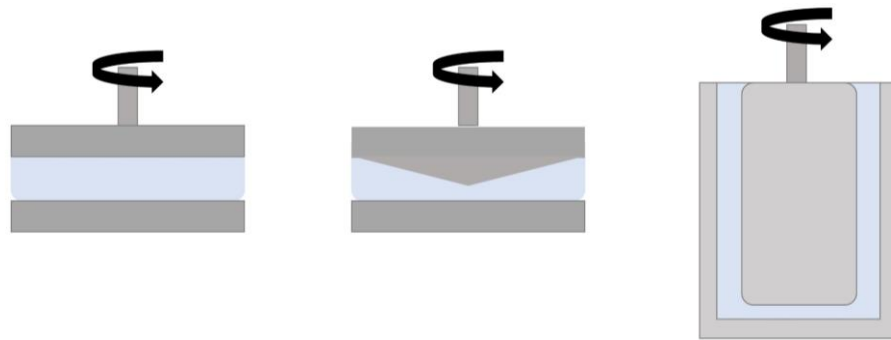


Figure 1.2 Rheometer geometry (a) Parallel plate (b) Cone and Plate (c) Concentric Cylinder

However, rheometric accessories such as cone and plate and parallel plate apply homogenous and non-homogenous strain on the sample respectively. In a parallel plate setup, the shear rate is zero at the centre and maximum at the edge of the plate (Equation 3).

$$\dot{\gamma} = \frac{\omega r}{L} \quad (3)$$

Polymers which are widely used to manufacture good for various applications are typically melted and processed in mixers and extruders to achieve the desired shape. Since the polymer is processed when it is in a molten stage, the determination of

rheological properties is to optimise the processing parameters. However, when used at a more sophisticated and advanced level, rheology can be used to understand deformations that occur on a molecular scale; for instance, rheometry has been used as a tool to link the macroscopic behaviour under deformation to molecular scale properties such as degree of branching, entanglement density and crystallisation kinetics⁷. Thus, change in rheological properties are sensitive to changes on a molecular level.

1.4 Spatial Temperature Gradient

Temperature gradients cause thermal stresses⁸ leading to irreversible deformations, flow of constituents⁹, and separation of components in a material¹⁰. The effect of temperature gradient on solids can be best understood by the thermoelastic effect which couples the resultant temperature field caused by deformation¹¹. The investigation of a gaseous mixture's behaviour under a thermal gradient began to separate isotopes of gases¹². In a gaseous mixture, a large mass difference between the constituents causes the heavier molecule to accumulate on the colder side of the gradient. However, this cannot be taken as a concrete rule as a change in behaviour can be observed if the mass concentration or temperature changes¹³.

In fluids, the application of a temperature gradient leads to a gradient in density and viscosity which affects the rheological properties and dynamics of the fluid. The effects of a temperature gradient on a liquid will be elaborated in further sections.

1.5 Coupled Heat Transfer and Fluid Flow

Rheology when coupled with external energy fields such as magnetic and electric gives rise to 'smart rheology' - electro-rheology¹⁴ and magneto-rheology¹⁵. This branch of rheology involves tuning rheological properties of 'smart fluids' by

exposing them to external electric or magnetic fields. These smart fluids have suspended nanoparticles such as iron, barium titanium oxalate which react to the external energy fields^{16,17}. Smart rheology has been eliciting renewed scientific interest due to their diverse applications in automotive industry and industrial processing of materials especially as shock absorbers and hydraulic valves. Despite their fascinating properties, smart fluids face several issues due to the nanoparticles settling out, inability to operate at very high/low temperatures and economically unviability.

Heat and fluid flow are more intimately coupled which can be understood by the Energy equation which investigates the increase in internal energy of the fluid due to the flow of a fluid in a non-isothermal temperature field. The cross effects of the dynamic coupling of the transport forces study the effect of flow on the heat transfer ability of the fluid and the effect of heat flow on the flow properties.

$$\frac{\partial T}{\partial t} + v_r \frac{\partial T}{\partial r} + \frac{v_\theta}{r} \frac{\partial T}{\partial \theta} + v_z \frac{\partial T}{\partial z} = k \left[\frac{1}{r} \frac{\partial}{\partial r} r \frac{\partial T}{\partial r} + \frac{1}{r^2} \frac{\partial^2 T}{\partial \theta^2} + \frac{\partial^2 T}{\partial z^2} \right] + \phi \quad (4a)$$

$$\begin{aligned} \phi = 2\mu & \left[\left(\frac{\partial v_r}{\partial r} \right)^2 + \left(\frac{1}{r} \frac{\partial v_\theta}{\partial \theta} + \frac{v_r}{r} \right)^2 + \left(\frac{\partial v_z}{\partial z} \right)^2 \right] \\ & + \mu \left[\left(\frac{1}{r} \frac{\partial v_r}{\partial \theta} + \frac{\partial v_\theta}{\partial r} - \frac{v_\theta}{r} \right)^2 + \left(\frac{1}{r} \frac{\partial v_z}{\partial \theta} + \frac{\partial v_\theta}{\partial z} \right)^2 \right. \\ & \left. + \left(\frac{\partial v_z}{\partial r} + \frac{\partial v_r}{\partial z} \right)^2 \right] \end{aligned} \quad (4b)$$

The conservation of energy (Equation 4) is one of the fundamental mathematical expressions that takes into consideration the heat carried by viscous fluids in motion. For an incompressible fluid with constant fluid properties, the energy equation in cylindrical co-ordinates¹⁸ can be written as Equation 4 which relates the rate of change in internal energy of a flowing fluid with conduction, convection and viscous dissipation of fluids⁶. Equation 4b elaborates the contribution of viscous dissipation.

Heat transfer within a flowing fluid with variable viscosity is irreversible. This results in entropy production within the system due to continuous energy exchange¹⁹. The temperature gradient affects fluid flow through rheological properties whereas flow properties affect heat flow through convection²⁰, viscous dissipation²¹ and diffusion²² which will be elaborated in the subsequent sections.

1.5.1 Thermal Convection

As discussed in Section 1.2, convection refers to the transfer of heat by the bulk motion of a non-isothermal fluid. When the fluid motion is the result of density differences, it is known as natural convection and if an external force such as pump or fan causes the fluid motion, it is called forced convection.

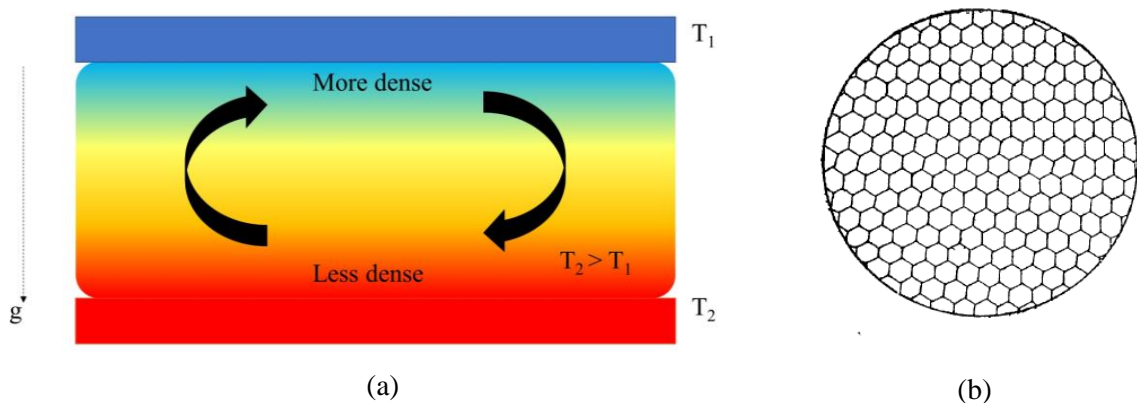


Figure 1.3 (a) Thermal Convection currents due to temperature and density gradient in a fluid heated from below (b) Hexagonal convection cells in water studied by Benard above a critical Rayleigh number²²

When a fluid is subjected to a vertical temperature gradient (heated from below), a resultant ‘top-heavy’ density and buoyancy gradient is setup (Figure 1.3a). Gravitational forces pull the fluid down which is balanced by the viscous damping within the fluid; this balance can be understood by studying the Rayleigh number (Ra).

$$Ra = \frac{g\beta\Delta TC_p\rho^2 L^3}{\mu k} \quad (5)$$

The Rayleigh number (Equation 5) contains strong information about the physics of heat transfer in convection flows. Above a critical Rayleigh number (Ra_c), heat transport is purely through conduction and the fluid is motionless. At values slightly higher than Ra_c , convection currents start setting in the fluid. A two-dimensional convection current is followed by three-dimensional currents, time dependent convection before finally becoming turbulent²³.

In unstable situations beyond Ra_c , the fluid rearranges itself into a uniform pattern called convection cells as seen in Figure 1.3b. The earliest experiments detailing this phenomenon was studied by Benard in 1901²⁴ and the theoretical foundations were laid down by Rayleigh in 1916²⁵. The critical Rayleigh number for stationary fluids is found to be ~ 1708 .

A coupling between natural convection and thermal conductivity of fluids has been studied by many authors. Numerical studies suggest that the heat transfer capacity and the onset of convection of fluids is sensitive to the power index n ²⁶. It was numerically found that the heat transfer capacity of a yield stress fluid increases for shear thinning fluids with $n < 1$ and vice versa for shear thickening fluids due to a change in the Rayleigh number; Ra increases with increase in n . Experimental results showed that the Ra_c changes by three orders of magnitude with change in yield stress of the fluid²⁷. The thermal conductivity also holds an inverse relationship with the fluid viscosity after a critical shear rate²⁸. One of the most fundamental ways in which fluid flow and heat transfer is related is through convection as it involves the bulk motion of a non-isothermal fluid.

1.5.3 Viscous Dissipation

Viscous dissipation or shear heating is the irreversible conversion of mechanical energy into heat. It occurs due to action of shear forces on adjacent layers of a fluid which is transformed into heat. The flow of fluids, especially high molecular weight polymers, leads to the generation of heat during processes such as extrusion, mixing and injection moulding²¹. Equation 4b takes shear heating/viscous dissipation into consideration.

Figure 1.4 is a qualitative representation of the effect of viscous dissipation on the fluid flow and temperature profile⁶. An increase in viscous dissipation of the fluid affects the temperature profile of the fluid depending on the local shear rate. This changes the viscosity profile of the material – the viscosity near the surface remains unchanged and the overall viscosity reduces due to an increase in temperature²⁹.

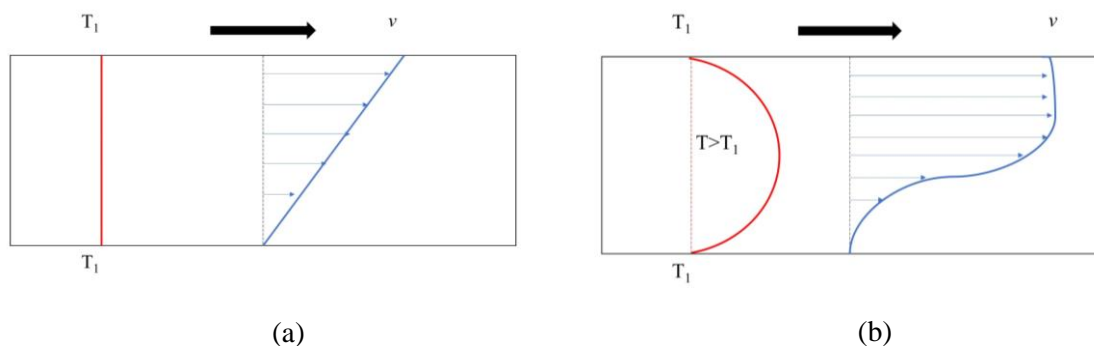


Figure 1.4 Qualitative comparison of temperature and velocity profile in drag flow (a) without viscous dissipation (b) with viscous dissipation; a non-linear temperature profile develops due to shear heating which subsequently affects the velocity profile

The effect of viscous dissipation on the temperature profile, viscosity and subsequently the fluid flow profile can be understood by the Brinkman Number (Equation 6). It is the ratio between the heat produced due to viscous dissipation of a fluid to the heat transported through conduction.

$$Br = \frac{\mu\dot{\gamma}^2L}{2k\Delta T} = \frac{\tau\dot{\gamma}L}{q} \quad (6)$$

In lower Br conditions *i.e.* lower shear rate, higher thermal conductivity and lower viscosity, the temperature profile across a temperature gradient is linear whereas an increase in Br causes the heat profile to be non-linear near the centre¹⁹. Viscous dissipation is a molecular phenomenon that details the effect of fluid flow on the temperature field of a fluid.

1.6 Thesis Outline

The effect of temperature on the rheological properties has been studied by many^{3, 6} whereas the inverse dependence of change in rheological properties such as viscosity and its effect on the thermal conductivity of a material especially non-Newtonian has been of increasing interest³⁰⁻³². The heat flux apparatus designed for this project will aid in understanding the effect of a spatial temperature gradient on the flow properties of a fluid since it can establish the required experimental conditions to investigate convection, viscous dissipation and thermodiffusion. This helps in understanding the overall coupling of heat flow and fluid flow irrespective of the nature of coupling present in the sample.

The and design of the heat flux apparatus and the materials used for apparatus fabrication is described in Chapter 2 along with the measurement and correction of heat flux data. It is followed by the validation of the apparatus in Chapter 3 by using a Newtonian fluid, here, glycerol. Once the apparatus is validated, the coupled transport dynamics of a non-Newtonian fluid is explored with the aid of Carbon nanotube nanofluid at two weight fractions. Chapter 5 serves as a conclusion and the future arenas of this particular research topic are laid out.

CHAPTER II

MATERIALS, METHODS AND DESIGN

2.1 Materials

The rheological characterisation was conducted on a shear stress-controlled rheometer equipped with an upper heated plate accessory (TA Instruments, New Castle, DE). The lower (stationary) portion of the rheometric system was customized with an in-house fabricated Peltier system. The relevant components of the Peltier system are: a recirculating chiller was purchased from PolyScience, IL, USA, a Pt-100 needle thermocouple was purchased from Omega, heat flux sensor (PHFS-01e) and heat flux data acquisition (DAQ) hardware was purchased from Fluxteq, VA, USA. Glycerol and single-walled carbon nanotubes (SWCNT) were procured from Alfa Aesar, MA, USA and CarboLex, PA, USA respectively. A Sonic Ruptor 400 system from Omni International, GA, USA was used to process SWCNT-glycerol suspensions.

2.2 Design of Heat Flux apparatus

The apparatus consists of two parallel plates (40 mm diameter) whose temperature control mechanisms are independent of each other that enables the temperature gradient establishment. A parallel plate setup was chosen to establish a uniform temperature gradient across the sample. Figure 2.1 illustrates a simple schematic of the system.

The top portion of the heat flux apparatus (Figure 2.2a) was an upper heated plate (UHP) geometry purchased from TA instruments. The UHP is heated by the rheometer via convective heating and the temperature is controlled through the TRIOS software. The lower portion was customized to incorporate the ability to impose a temperature gradient on the sample.

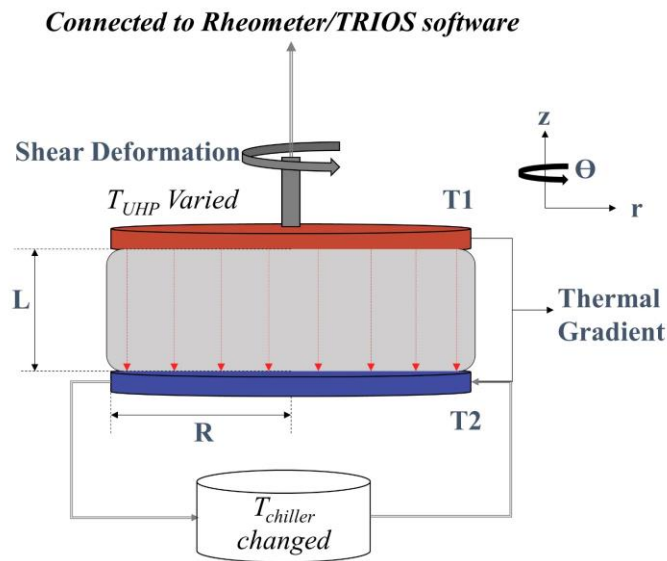


Figure 2.1 Schematic of Heat Flux Apparatus system outlining orthogonal superimposition of temperature gradient and shear deformation; T_{UHP} is controlled by the rheometer through convective heating, T_{LHP} is controlled through recirculating chiller

As seen in Figure 2.2b, the test plate and Peltier plate of the lower heated plate (LHP) were fabricated from stainless steel (Grade 316) and aluminium (6061-T6) respectively which was housed in Teflon for insulation. A recirculating chiller was used for controlling the temperature of the LHP which was measured by needle thermocouple inserted in the Test Plate right below the test surface.

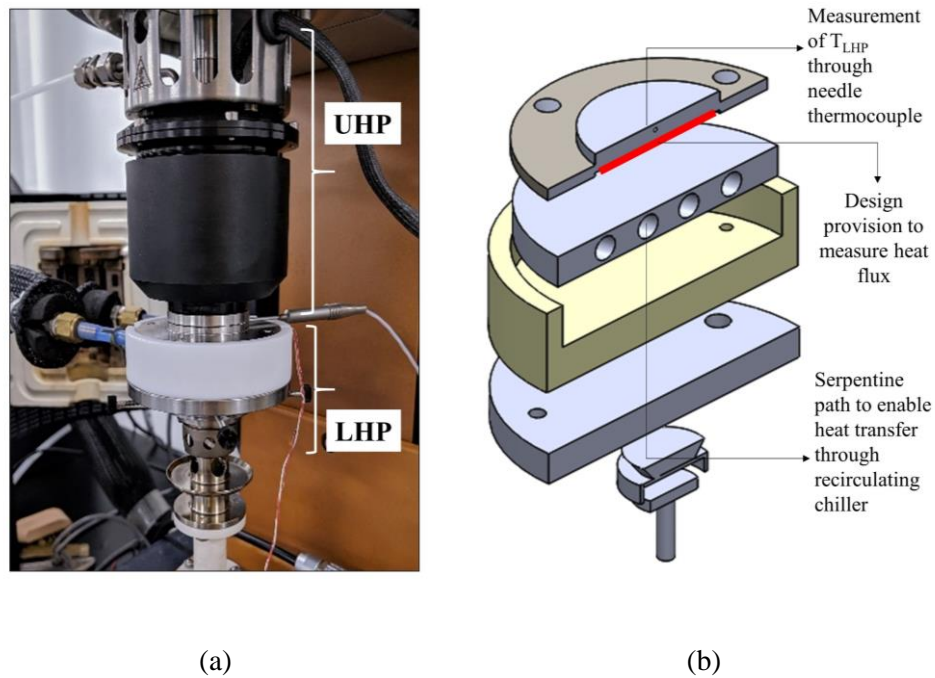


Figure 2.2 (a) Heat Flux apparatus consisting of UHP and LHP (b) Section view of LHP components (Test Plate, Peltier Plate, Teflon Insulation and Mount) with description of salient features

2.3 Establishing Temperature Gradient

The temperature gradients were set up by keeping the LHP temperature (T_{LHP}) constant and varying the UHP temperature (T_{UHP}) as shown in Figure 2.3 which elaborates the mechanism for T_{LHP} 35°C. The input heat load to the UHP and LHP were controlled to achieve the desired gradient.

The achievable temperature gradients range from -16K/mm to 30K/mm. Temperature gradients are calculated according to Equation 7; thus, gradients concurrent with gravity are assigned positive and counter to gravity are assigned negative.

$$\text{Temperature Gradient } \nabla T = \frac{T_{UHP} - T_{LHP}}{L} \quad (7)$$

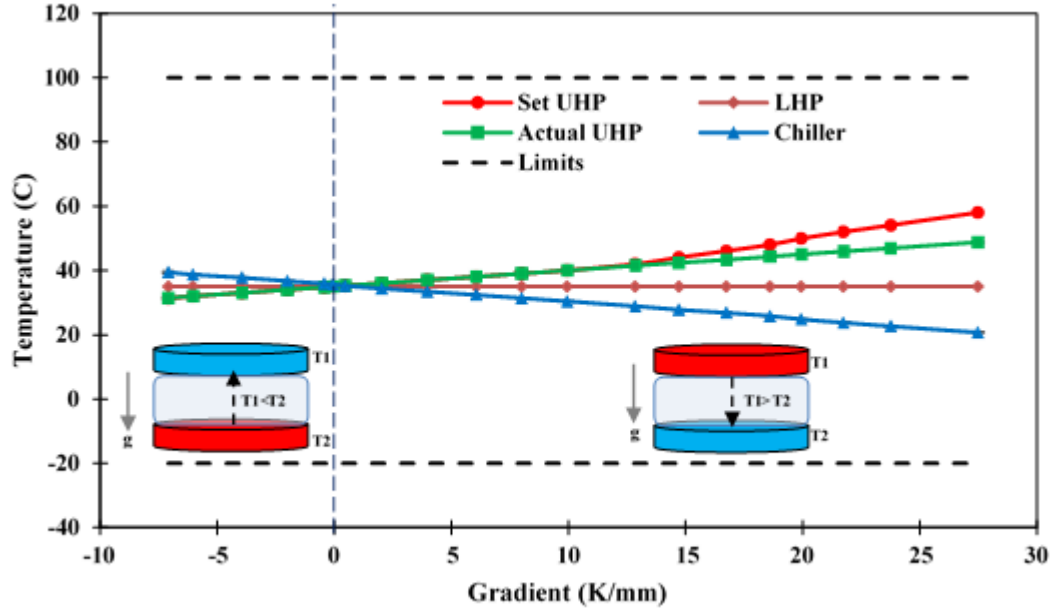


Figure 2.3 Sample Performance Curve for glycerol at T_{LHP} 35°C; temperature gradients along the direction of gravity were designated positive and vice-versa

2.4 Heat Flux Measurement and Analysis

The heat flux was measured using a differential thermopile heat flux sensor (Figure 2.4a inset). The thickness of the sensor was 600 μ m. It was embedded between the test plate and Peltier plate as mentioned in Figure 2.2b. The thickness of the engineered slot for the heat flux sensor was \sim 1.1 mm (Figure 2.4b). Data from the heat flux was logged using a data acquisition system (DAQ) as seen in Figure 2.4a. The raw voltage output by the sensor was converted to heat flux by calculating the sensitivity (Se) of the sensor which changes linearly with the temperature of the sensor (Equation 8). The equation to calculate the sensitivity was provided by the supplier (Equation 8b).

$$q = \frac{\Delta V}{Se} \quad (8a)$$

$$Se = [0.00334(T_{\circ C}) + 0.917] * 1.15 \quad (8b)$$

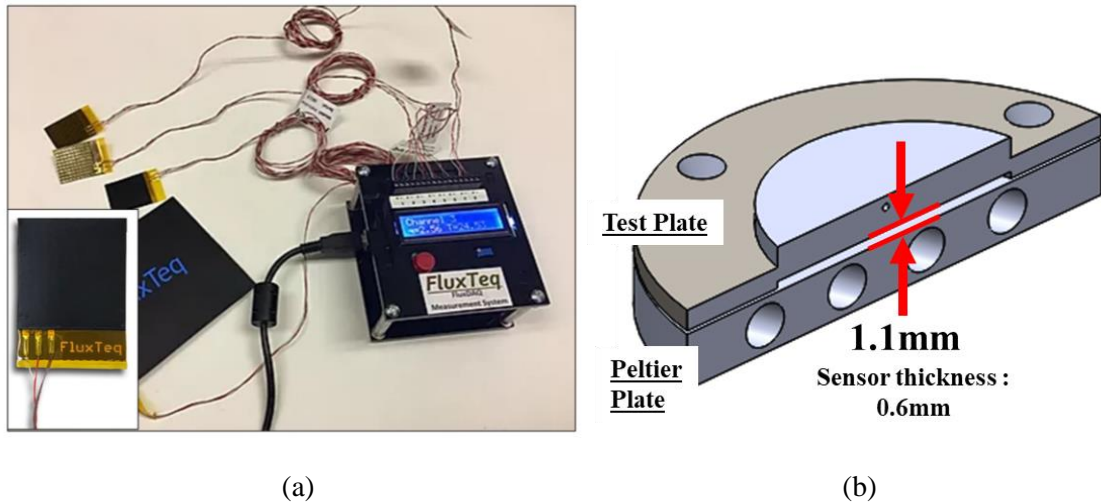


Figure 2.4 (a) Heat Flux measurement accessories from Fluxteq; Data Acquisition system for measurement of heat flux (Inset) Heat Flux sensor PHFS-01e (b) Thickness of engineered slot in between Test and Peltier Plate for heat flux sensor

Since the slot for the sensor was 1.1mm in thickness and the sensor was 0.6mm, there was an air gap in the heat transfer path which increased the thermal resistance of the heat flux apparatus. Since the slot for the sensor was 1.1mm in thickness and the sensor was 0.6mm, there was an air gap in the heat transfer path which increased the thermal resistance of the heat flux apparatus.

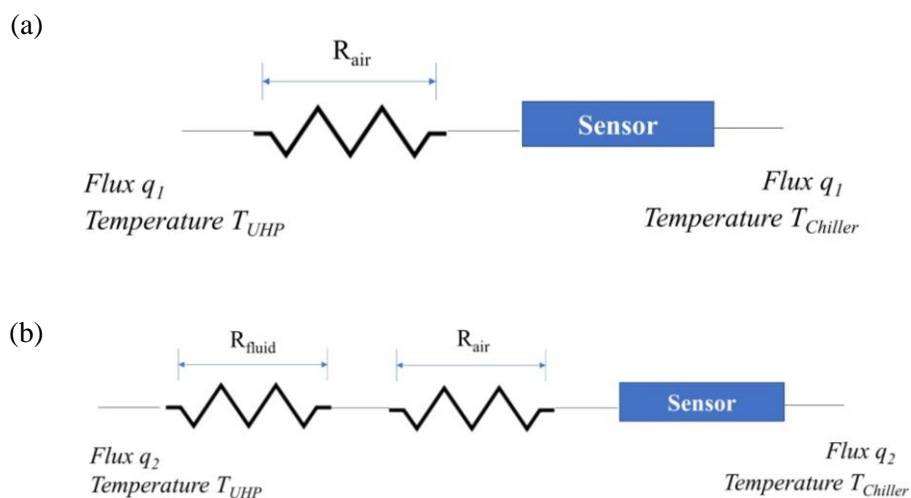


Figure 2.5 Thermal circuit diagram of the heat flux apparatus (a) flux q_1 without fluid sample between UHP and LHP (b) q_2 with fluid sample between UHP and LHP

Experiments were conducted without the fluid sample between the UHP and LHP (the plates were kept in contact) to ascertain the flux in the system; the flux was denoted as q_1 . In this thermal circuit (Figure 2.5a), the system has two resistors – air and sensor. Similarly, when there is fluid in between the LHP and UHP, it serves as an additional resistance in the circuit (Figure 2.5b); this flux is denoted as q_2 . At a constant ΔT , an increase in thermal resistance causes a decrease in heat flux values, thus $q_1 > q_2$. Since the resistors are in series, Equation 9a can be used to calculate the combined heat transfer in the circuit.

$$\Delta T = q \sum R \quad (9a)$$

$$\Delta T = q_1(R_{air} + R_{sensor}) \quad (9b)$$

$$\Delta T = q_2(R_{air} + R_{fluid} + R_{sensor}) \quad (9c)$$

Equations 9b and 9c were equated to obtain the values of the thermal resistance of fluid (R_f) by equation 10a and subsequently, the thermal conductivity of glycerol (Equation 10b).

$$R_{fluid} = (R_{sensor} + R_{air}) \left[\frac{q_1}{q_2} - 1 \right] \quad (10a)$$

$$k_{glycerol} = \frac{L}{\pi R^2 * R_{fluid}} \quad (10b)$$

2.5 Rheological Characterisation

Isothermal tests were conducted in an Environmental Test Chamber (ETC) under shear sweep conditions. The equilibration time for each shear rate was 90s followed by a sampling time of 30s.

Rheological tests under temperature gradients were conducted at constant shear rates (flow peak holds). The gap between the plates was maintained at 500 μ m (L).

The temperature of LHP was stabilised at the desired set point and the gap was zeroed to ensure stability of gap at every temperature gradient at that T_{LHP} . The thermal expansion coefficient of the UHP was taken into account by the TRIOS software to ensure a uniform gap throughout experiments at different temperature gradients.

The tests were conducted for a total strain of ~ 500 at each shear rate (except 100 s^{-1}) and the test duration for each shear rate is explained in Table 2. The measured viscosity was averaged over the duration of the test for each shear rate. Three test results at each shear rate and temperature gradient was averaged to obtain the final viscosity.

Shear Rate (1/s)	Strain	Time (s)
0.5	502.5	1005
1	502	502
5	500	100
10	500	50
100	5000	50

Table 2 Shear rates tested and corresponding sample time

CHAPTER III

HEAT FLUX APPARATUS VALIDATION

3.1 General Introduction

The heat flux apparatus was validated by studying the coupled dynamics of heat and fluid flow of a Newtonian fluid. Glycerol was chosen as the model fluid for validation. Validating the experimental apparatus and technique using glycerol simplifies the validation process due to the shear rate-independent rheological properties characteristic of a Newtonian fluid.

Glycerol is a tribasic alcohol which is colourless, odourless, viscous liquid. with diverse uses as a lubricant, softener, desiccant and plasticizer³³. It has also been extensively studied from both the viewpoints of rheology^{34,35} and heat transfer^{36,37}. The non-volatile nature of the fluid lends stability to glycerol as a rheometric sample throughout the duration of the test and helps in reducing errors.

The validation of the heat flux apparatus can be divided into two parts – rheological and thermal. The rheological properties of glycerol under a spatial thermal non-equilibrium is analytically modelled by extending the rheological properties under isothermal conditions to non-isothermal boundary conditions. The model values calculated analytically are compared with the experimentally obtained viscosity values to validate the rheological aspect of the heat flux apparatus. The thermal aspect of the

heat flux apparatus is validated by numerically solving for the thermal conductivity of glycerol and heat flux through the sample under a temperature gradient and comparing it with the experimentally measured values. The Brinkman number (Equation 6) and Richardson number were used to understand the coupled transport dynamics of the system and validate the technique.

3.2 Temperature Gradients established

Glycerol was tested at three constant LHP temperatures – 35°C, 40°C and 45°C (Figure 3.1). These specific temperatures were chosen for operational ease.

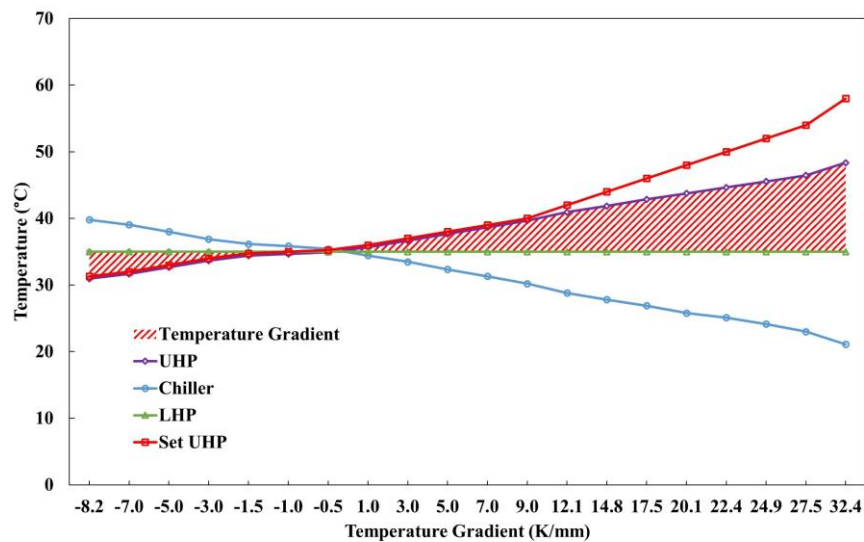


Figure 3.1 Established temperature gradients for glycerol at constant T_{LHP} : 35°C; temperature gradients were established by keeping T_{LHP} constant and varying T_{UHP} .

The temperature gradient was established according to the protocol mentioned in Section 2.3. At higher temperature gradients, the actual UHP temperature was lower than the Set UHP due to the heat load from the LHP which was maintained at a much lower temperature.

The display temperatures of UHP and chiller were corrected for zero error using the reported flux as a guide. The display temperature was plotted against the reported flux; the intercept on the y axis represents the display temperature at zero flux. The gap between the intercept and desired temperature is used to correct the zero error at each established gradient.

3.3 Validation – Rheological

3.3.1 Glycerol under isothermal conditions:

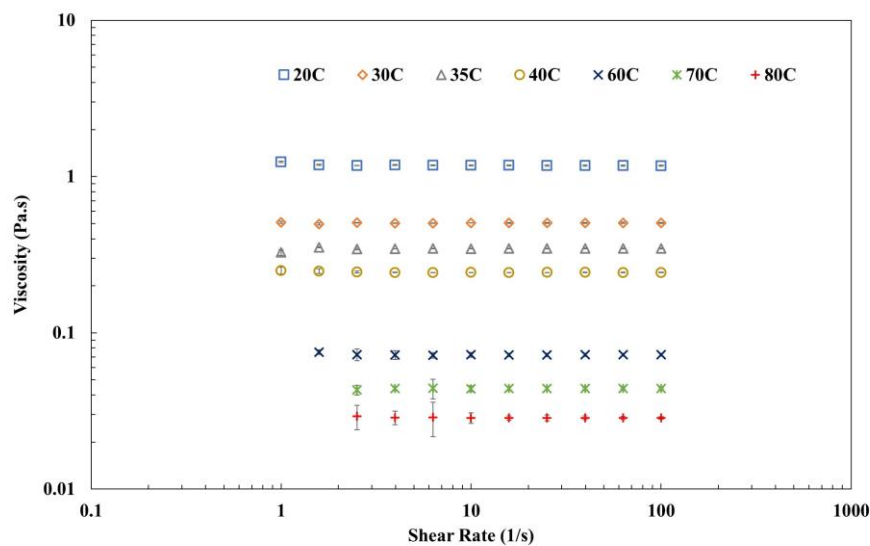


Figure 3.2 Viscosity of glycerol in ETC at isothermal conditions across shear rates ranging from 1 s^{-1} to 100 s^{-1}

To understand the behaviour of glycerol under a thermal non-equilibrium, it was essential to investigate its behaviour under isothermal conditions and then apply non-isothermal boundary conditions to the energy equation to extrapolate the dataset. The viscosity of glycerol is measured across a range of shear rates (1 s^{-1} to 100 s^{-1}) at different temperatures. The fluid exhibits Newtonian behaviour across the tested shear rates and a fall in viscosity can be observed with increase in temperature (Figure 3.2).

The viscosity-temperature relationship of glycerol follows an inverse exponential trend³⁸ that can be understood by Equation 11.

$$\mu(T) = Ae^{B/T} \quad (11)$$

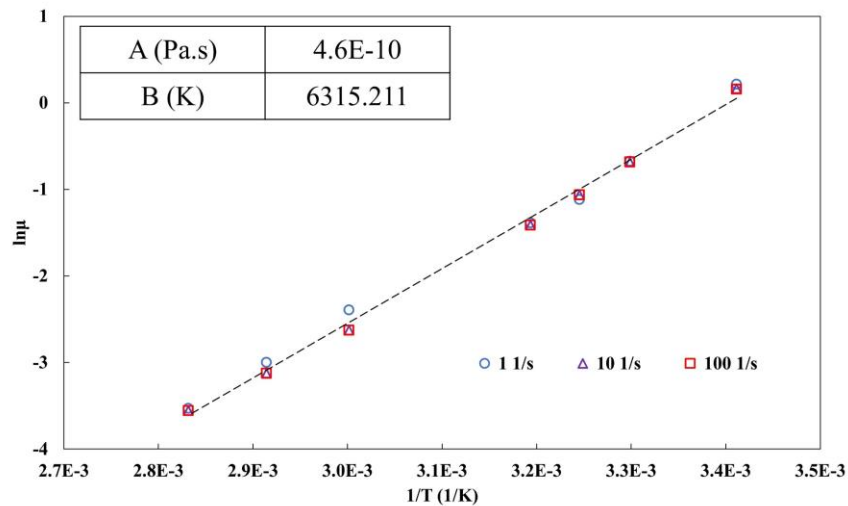


Figure 3.3 $\ln \mu$ vs. $1/T$ for glycerol tested at 1 s^{-1} , 10 s^{-1} and 100 s^{-1} (Inset) Fit parameters: A, B

The fit parameters A and B are determined by plotting Figure 3.2 in the form of $\ln \mu$ vs. $1/T$ and calculating the intercepts and slopes of the resultant graph (Figure 3.3). The Newtonian behaviour of glycerol is further confirmed in Figure 3.3 by the superimposition of data points for different shear rates.

3.2.2 Viscosity under temperature gradients – Analytical Model:

The rheological behaviour of glycerol under the established temperature gradients was mathematically modelled using Energy equation (Equation 4a) and the isothermal viscosity-temperature relationship (Equation 11). Equation 4b is used to calculate the viscous dissipation contribution to the energy equation.

Incorporation of steady state, symmetricity in θ direction, stable interface, impermeable plate and uniform temperature distributions along the plate surface (Equation 12) assumptions reduce Equation 4a to Equation 13.

$$\frac{\partial}{\partial t} = \frac{\partial}{\partial \theta} = v_z = v_r \frac{\partial T}{\partial r} = \frac{\partial T}{\partial \theta} = 0 \quad (12)$$

$$k \left[\frac{d^2 T}{dz^2} \right] + \mu \left[\left(\frac{\partial v_\theta}{\partial r} - \frac{v_\theta}{r} \right)^2 + \left(\frac{\partial v_\theta}{\partial z} \right)^2 \right] = 0 \quad (13)$$

Velocity in the θ direction for a parallel plate setup is analytically obtained from the shear rate equation for parallel plate setup. (Equation 3). Integrating the resultant energy equation leads to the temperature profile of the fluid between the two plates of the rheometer which are maintained at different temperatures.

$$T = \frac{\mu(T)\dot{\gamma}^2 L^2}{2k\Delta T} \left(\frac{z}{L} \right) - \frac{\mu(T)\dot{\gamma}^2 L^2}{2k\Delta T} \left(\frac{z}{L} \right)^2 + \Delta T \left(\frac{z}{L} \right) + T_1 \quad (14)$$

Equation 11 and 14 are numerically solved to obtain the viscosity of glycerol under established temperature gradients at three constant LHP temperatures – 35°C, 40°C and 45°C (dashed lines in Figure 3.4).

The viscosity of glycerol falls with an increase in temperature gradient (from negative to positive) at a constant T_{LHP} . A fall in viscosity is also observed with an increase in T_{LHP} at a constant temperature gradient. Glycerol exhibits Newtonian behaviour under a spatial thermal non-equilibrium as seen in Figure 3.4 *i.e.* the viscosity of glycerol does not change with shear rate under an imposed temperature gradient.

3.2.3 Viscosity under temperature gradients – Experiment:

The heat flux apparatus was used to establish temperature gradients across a rheometric sample. As mentioned in Section 2.4, the plates of the rheometer are maintained at different temperatures to establish the desired gradient.

Glycerol was tested at 3 different TLHP – 35°C, 40°C and 45°C. As soon as the temperature gradient was established, a constant shear rate was applied and the viscosity was recorded. Simultaneously, the heat flux was also measured and logged.

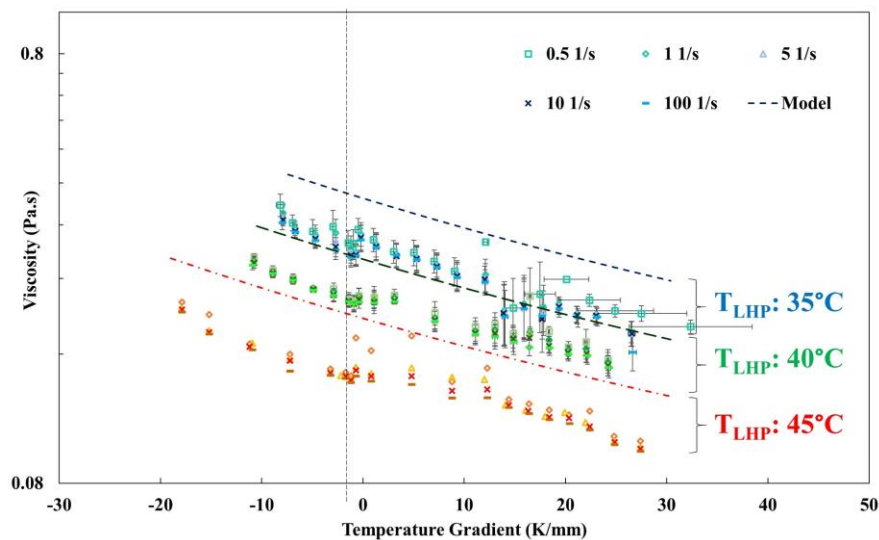


Figure 3.4 Viscosity vs. Temperature gradients at T_{LHP} 35°C, 40°C and 45°C; comparison between analytical model (dotted line) and experimental results (discrete points)

As seen in Figure 3.4 viscosity falls with an increase in temperature gradient from negative to positive at a constant T_{LHP} . The viscosity also falls with an increase in T_{LHP} at a constant temperature gradient.

The viscosity values predicted by the analytical model are higher than the experimentally obtained ones at all three T_{LHP} . However, they fall within the same order

of magnitude and follow a similar trend of decrease in viscosity values with increase in temperature gradient.

3.2.4 Isothermal viscosity comparison – ETC vs Heat Flux Apparatus

To investigate the gap between the model and experimental values of viscosity under a temperature gradient, the viscosity values under isothermal conditions at 35°C, 40°C and 45°C obtained from the ETC and Heat Flux Apparatus were compared (Figure 3.5).

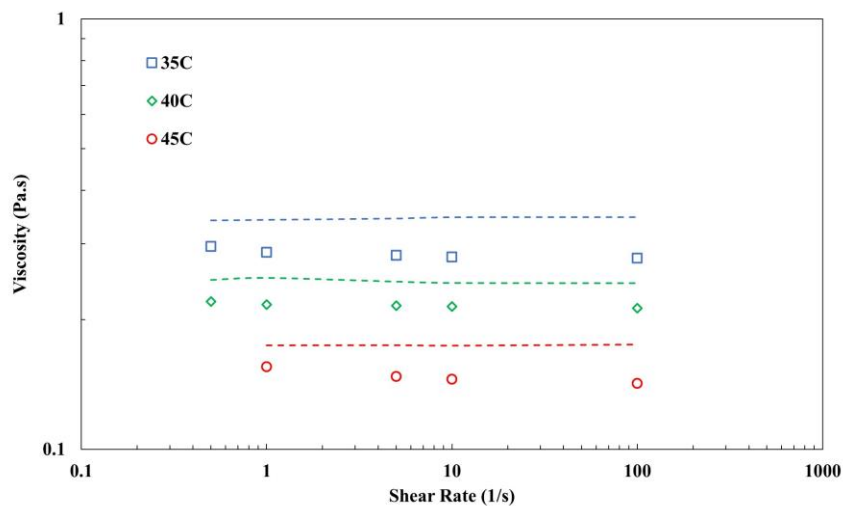


Figure 3.5 Viscosity values at isothermal conditions measured in the ETC (dashed line) and Heat Flux Apparatus (Discrete points) at 35°C, 40°C and 45°C

As seen in Figure 3.5, the viscosity values obtained from the ETC are higher than the values obtained from the heat flux apparatus. This gap between the viscosity values have caused the gap between the model and experimental values as seen in Figure 3.4.

3.3 Validation - Thermal

3.3.1 Experimental thermal conductivity of glycerol under temperature gradient:

The heat flux measured by the heat flux sensor was corrected for the presence of air according to the protocol mentioned in Section 2.3. The corrected thermal conductivity and heat flux values were compared with values previously reported in literature⁵.

$$k = M + NT + PT^2 \quad (15)$$

$$M = 0.2837; N = -2.12E - 05; P = 1.5963E - 07$$

The thermal conductivity of glycerol can be obtained by Equation 15. To calculate the value of k from Equation 15, an arithmetic average of LHP and UHP temperature is used as temperature.

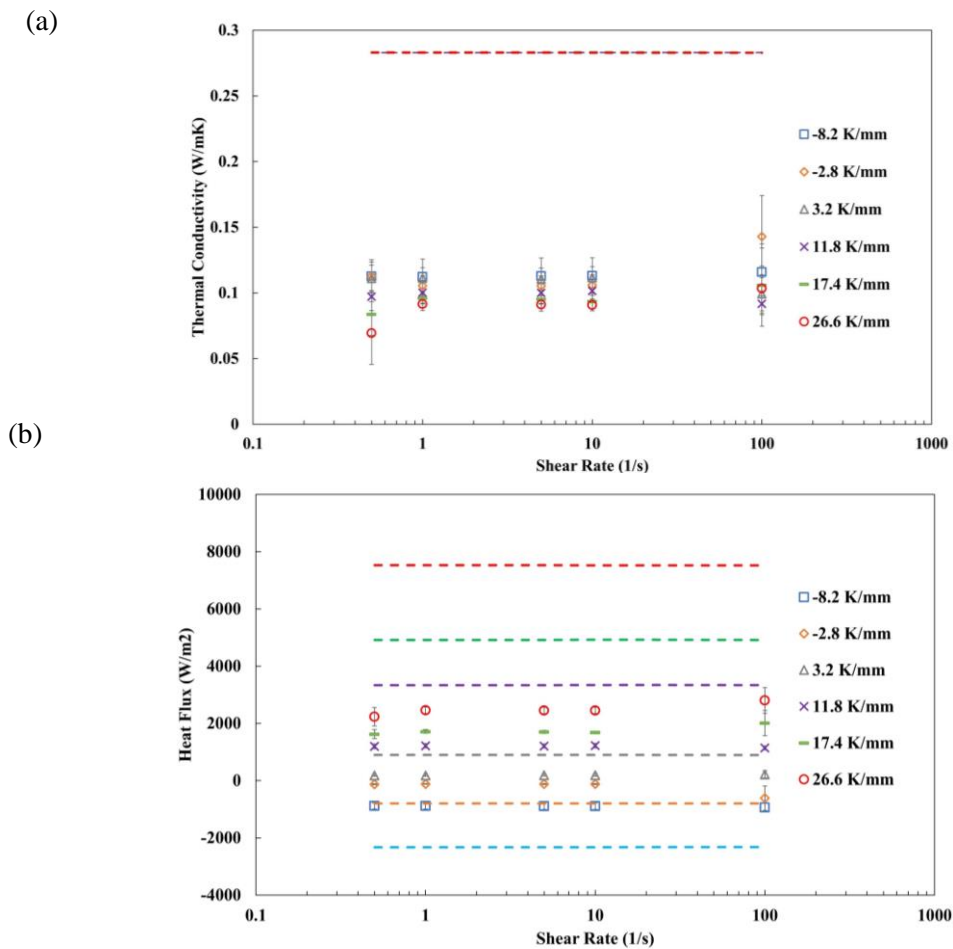


Figure 3.6 Comparison between values reported in literature (dotted line) and experimental values (discrete points) at $T_{LHP} 35^\circ\text{C}$ (a) Thermal conductivity of glycerol vs. shear rate (b) Heat flux vs. shear rate

As seen in Figure 3.6, the experimental thermal conductivity and absolute heat flux value was lower than the values reported in literature. This gap in thermal properties can be bridged by perfecting the correction protocol for the presence of air gap.

3.4 Validation Curves

The Brinkman Number was chosen to validate the technique since it combines the shear and heat flow dependent properties. The relationship of Br with temperature gradient and the square of shear rate was probed. As observed from Equation 6, the relationship between the square of shear rate should yield an exponent of 1 whereas the dimensionless parameter holds an inverse power relationship with the temperature gradient. Figure 3.7 elaborates the relationship between the experimental Br with the square of shear rate for a select few temperature gradients at T_{LHP} 35°C (others not shown for brevity).

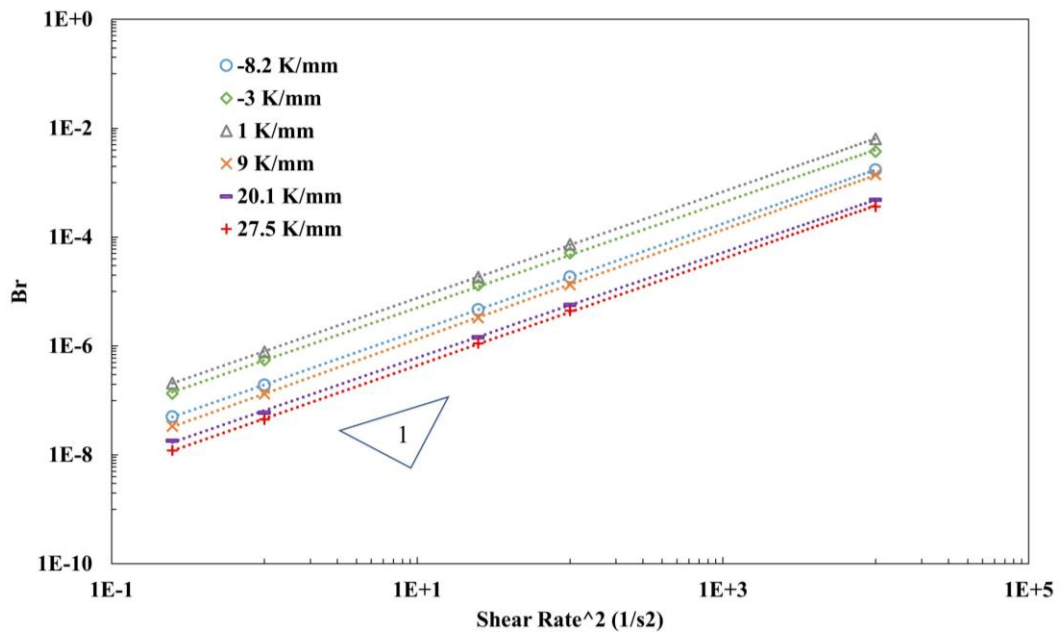


Figure 3.7 Experimental Brinkman number vs $\dot{\gamma}^2$ of select temperature gradients at T_{LHP} 35°C; the experimental Br exhibits an exponent of 1 with $\dot{\gamma}^2$ which is represented by the right triangle

The inset which presents the slope/exponent of the power relationship at all tested T_{LHP} shows that the experimental Br exhibits a slope of 1. This validates the behaviour of the apparatus.

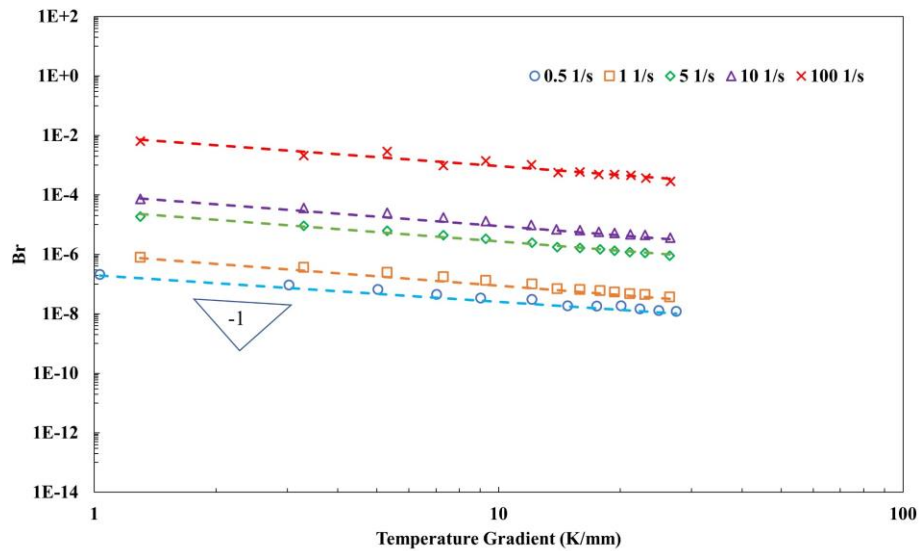


Figure 3.8 Experimental Brinkman number vs. temperature gradient of tested shear rates at T_{LHP} 35°C (only positive gradients shown to enable logarithmic representation); the experimental Br exhibits an exponent of -1 with temperature gradient which is represented by the right triangle

Similarly, Figure 3.8 explores the relationship of experimental Br with the temperature gradient at the tested shear rates for T_{LHP} 35°C (others not shown for brevity). An inverse exponential trend is observed between the two parameters. The inset which exhibits the slope/exponent shows that the parameters are related to each other by a power of -1. This validates the behaviour of the apparatus.

3.5 Scaling of the experiment

The technique was scaled with the help of two dimensionless numbers – Brinkman and Richardson number (equation 17). Scaling the experiment with the help of dimensionless numbers helps in understanding the transport dynamics of fluid and

heat flow from a holistic point of view. It encompasses all the problems that belong to the same class of transport forces by allowing for data reduction³⁹.

The physical significance of the Brinkman number has been discussed in Section 1.5.3. The Richardson number allows the coupling of shear rate and temperature gradient on the x axis whereas the Brinkman number helps in mapping the viscosity and heat flux on the y axis.

$$Ri = \frac{g\beta\Delta T}{\dot{\gamma}^2 L} \quad (17)$$

Figure 3.9 scales the coupled dynamics of heat flow and fluid using Br and 1/Ri. and the following relationship can be inferred:

$$Br = \delta Ri^\varepsilon \quad (18)$$

From a power fit of the experimental results till a Ri value of 0.1, it was determined that $\delta = 5E-6$ and $\varepsilon = -0.9173$.

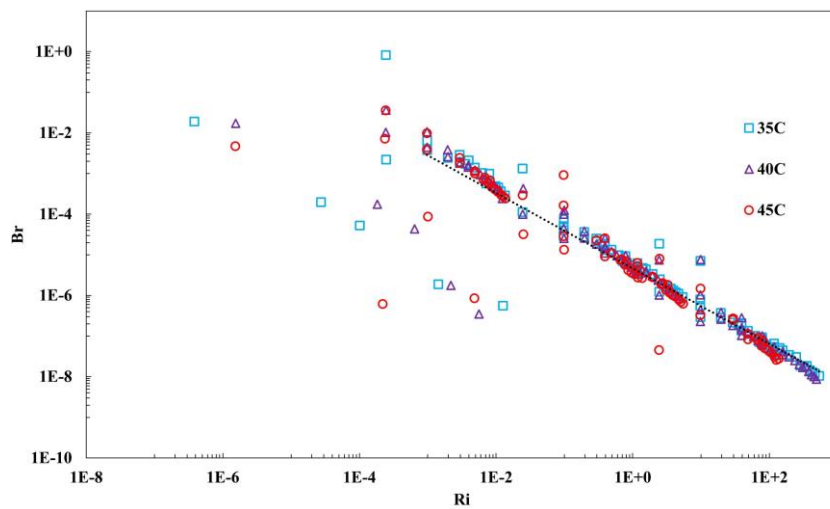


Figure 3.9 Scaled transport dynamics of coupled heat and fluid flow (Br vs. Ri) at T_{LHP} : 35°C, 40°C and 45°C; the experimental data measured at all TLHP at several temperature gradients and lower to intermediate shear rates collapse on a single curve which is fit to a power curve

3.6 Discussion

The coupled transport dynamics of heat and fluid flow in Newtonian fluids was presented in Chapter 3 along with the validation protocol of the technique. It was found that the flow properties (viscosity) is affected by temperature gradient whereas for Newtonian fluids, the thermal properties (heat flux) is not affected by shear. The apparatus was validated using the Brinkman number and investigating the relationship of Br with $\dot{\gamma}$ and ∇T .

The experimental data obtained at a range of shear rates and temperature gradients was nondimensionalised using Br and Ri which enabled the collapsing of data on a single curve. The significance of the experimental data collapsing on a single straight line gives the observer an insight into the cross coupled phenomena occurring across the range of tested temperature gradients and shear rates except at lower ranges of Ri where a scatter in data points is observed.

Br ranges from 10^{-9} to 10^{+1} whereas Ri ranges from 10^{-8} to 10^{+2} ., thus, most of the experimental data lies in the low to intermediate shear region.

From Figure 3.9, it can be inferred that Br is approximately proportional to Ri^{-1} *i.e.*

$$BrRi = 5 \times 10^{-6} \quad (19)$$

By using equation 19, the Brinkman number of the system can be obtained which delves into the comparison of shear contribution and heat conduction to the heat transfer. In the lower Ri regime, *i.e.* a low shear and high temperature gradient regime, a higher Br is observed which can be linked to a higher entropy generation rate¹⁹.

Since the linearity of Br with Ri starts scattering at lower Ri (higher shear rates or lower temperature gradients), these regimes can be investigated further to understand

the deviation from linear trend. This data set serves as a preliminary study on the scaled transport processes that couple fluid and heat flow.

CHAPTER IV

EXTENSION TO NON-NEWTONIAN FLOW REGIMES

4.1 General Introduction

The addition of nanoparticles to a base fluid matrix leads to fascinating properties being exhibited by the resultant suspension. The advantages and potential applications of dispersing particles in a base fluid matrix has been studied extensively by several authors^{40–42}. The effect of suspending nanoparticles in common heat transfer fluids such as ethylene glycol, water and glycerol on the heat transfer abilities of the resultant suspension was studied and a non-linear increase in the effective thermal conductivity of the nanofluid with volume fraction of nanoparticles was observed^{43–45}. This has led to great scientific interest in these materials due to their potential application as heat transfer fluids⁴⁶. Amongst the various nanoparticles, carbon nanotubes (CNTs) gained wide spread attention due to their exceptional electrical, thermal and physical properties⁴⁷.

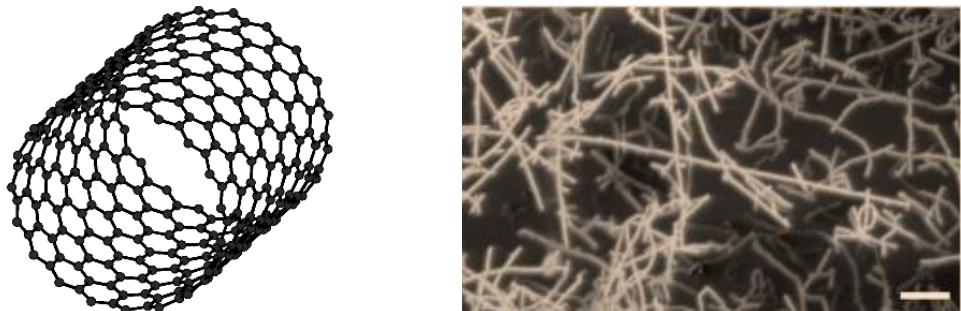


Figure 4.1 (a) Structure of Single Wall Carbon Nanotube⁴⁹ (b) SEM micrograph of Single Wall Carbon nanotube⁵⁰

CNTs are tubular particles made entirely of carbon whose diameter is in the nanometre range (Figure 4.1). The length of the tube can be varied to obtain a range of thermo-mechanical properties⁴⁸. CNT nanofluids have diverse uses in in the field of microelectronics, material science, biotechnology and medicine.

Figure 4.1a shows the graphic illustration of a SWCNT particle whose diameter is in the nanometre range. The illustration was taken from Burke *et al*⁴⁹. Figure 4.1b displays a SEM micrograph of SWCNT particles which was published by Homma *et al*⁵⁰. Addition of carbon nanotubes (CNTs) to common fluids such as water, ethylene glycol, glycerol and silicone oil specifically alters the rheological and thermal properties of the nanofluid compared to the base fluid^{51, 52}.

For instance, the incorporation of carbon nanotubes in pure glycerol changes several key properties of the base fluid – both rheological and thermal. The rheological properties of glycerol are Newtonian as discussed extensively in Chapter 3, and addition of CNT changes the rheological behaviour to non-Newtonian, specifically shear-thinning³³.

From the perspective of heat transfer abilities, an increase in the effective thermal conductivity has been observed with an increase in volume fraction of CNT added to glycerol⁵³. An increase in viscosity and electrical conductivity is also observed with increase in CNT volume fraction^{54, 55}.

Even though addition of CNTs leads to enhancement of thermal and other physical properties, they are notorious for their tendency to aggregate and agglomerate within the liquid media which leads to an unstable suspension⁵⁶. Thus, sample preparation is key to extract maximum usage from CNT in liquid media.

Nanofluids are prepared through predominantly two routes – one step method and two step method. The one-step method involves simultaneously making and dispersing the nanoparticles in the base fluid whereas in the two-step method, the nanoparticles are initially prepared as a dry powder followed by their dispersion in the fluid matrix. The former leads to more stable suspensions whereas the latter is a relatively economic method⁵⁷.

One of the most commonly used physical tools for breaking CNT aggregates and stabilising nanofluid suspensions is ultrasonication which involves irradiating a suspension with sound energy (> 20kHz) that aids in agitating and breaking down particle agglomerates within the fluid⁵¹. Studies suggest that an increase in ultrasonication time and power leads to an increase in viscosity and thermal conductivity of the nanofluid which is attributed Brownian motion and interparticle potential of the nanoparticles⁵⁸.

4.2 Sample Preparation

Nanofluid suspensions of 0.5 and 1 weight% CNT in glycerol (denoted as N0.5 and N1 respectively) were prepared using the two-step method. A probe indicator (Omni Ruptor 400) was used to ultrasonicate the suspensions at a power of 160 W for 120 minutes. The sonication was performed in pulse mode at 60% (sonication for 1.2s followed by 0.8s rest).

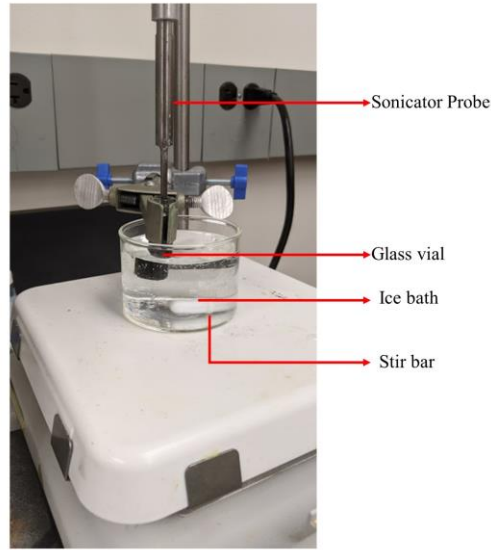


Figure 4.2 Setup for ultrasonication of CNT nanofluid; the glass vial containing the nanofluid was suspended in an ice bath to control temperature rise during ultrasonication

The vial was suspended in an ice bath with a magnetic stirrer to control the temperature rise of the sample due to viscous heating caused by the high shear rates during ultrasonication (Figure 4.2). Post sonication, the vial was kept stationary for 17 hours and no phase separation was visible in the suspension.

4.3 Temperature Gradients Established

N0.5 and N1 were tested at a constant LHP temperature of 35°C. The temperature gradients ranged from -7.8 K/mm to 3.2 K/mm for N0.5 and -9 K/mm to 3 K/mm for N1 nanofluid as seen in Figure 4.3. Similar to glycerol, the temperature of the LHP was maintained constant and the gradients were established by varying the temperature of the UHP.

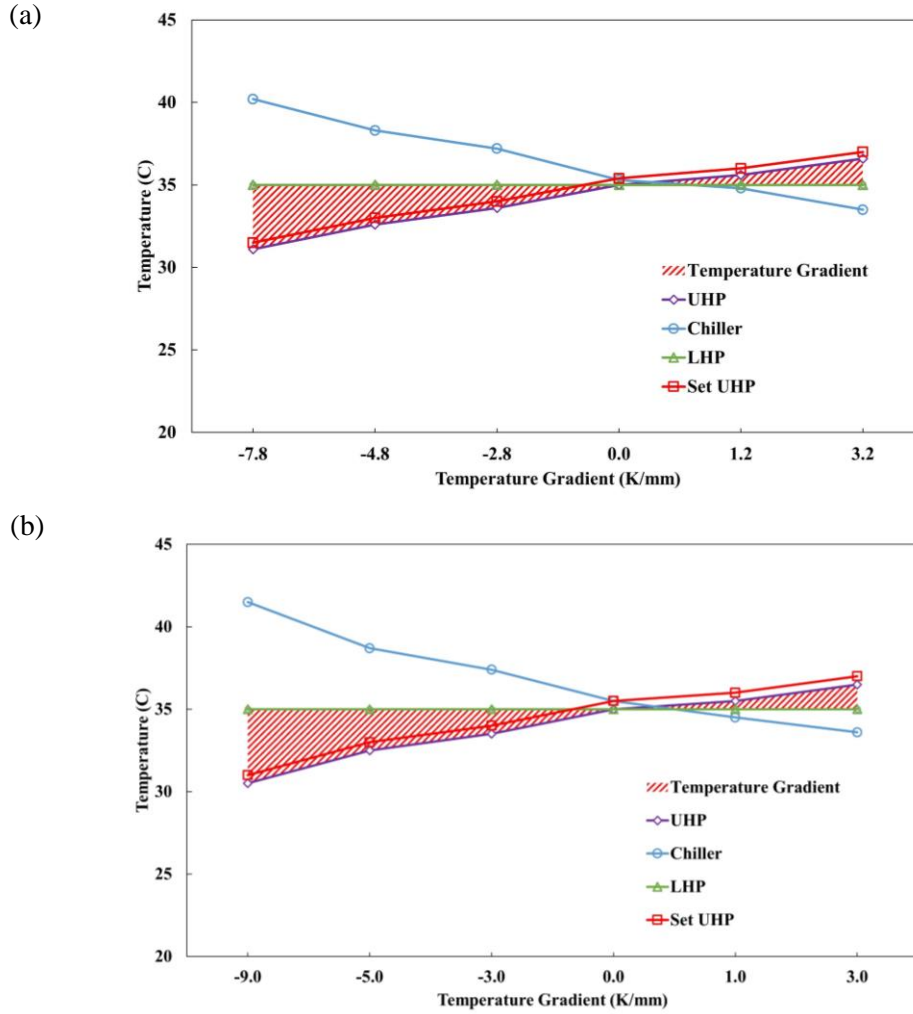


Figure 4.3 Established temperature gradients at T_{LHP} 35°C (a) N0.5 (b) N1

4.4 Rheological Properties of CNT in glycerol nanofluid

4.4.1 Nanofluids under isothermal conditions

Similar to pure glycerol, N0.5 and N1 were tested under isothermal conditions at a range of shear rates (1 s^{-1} to 10 s^{-1}) to extrapolate their coupled dynamics under a temperature gradient. They exhibit a shear thinning profile in the range of tested shear rates and temperatures (Figure 4.4). There was negligible change in viscosity between N0.5 and N1.

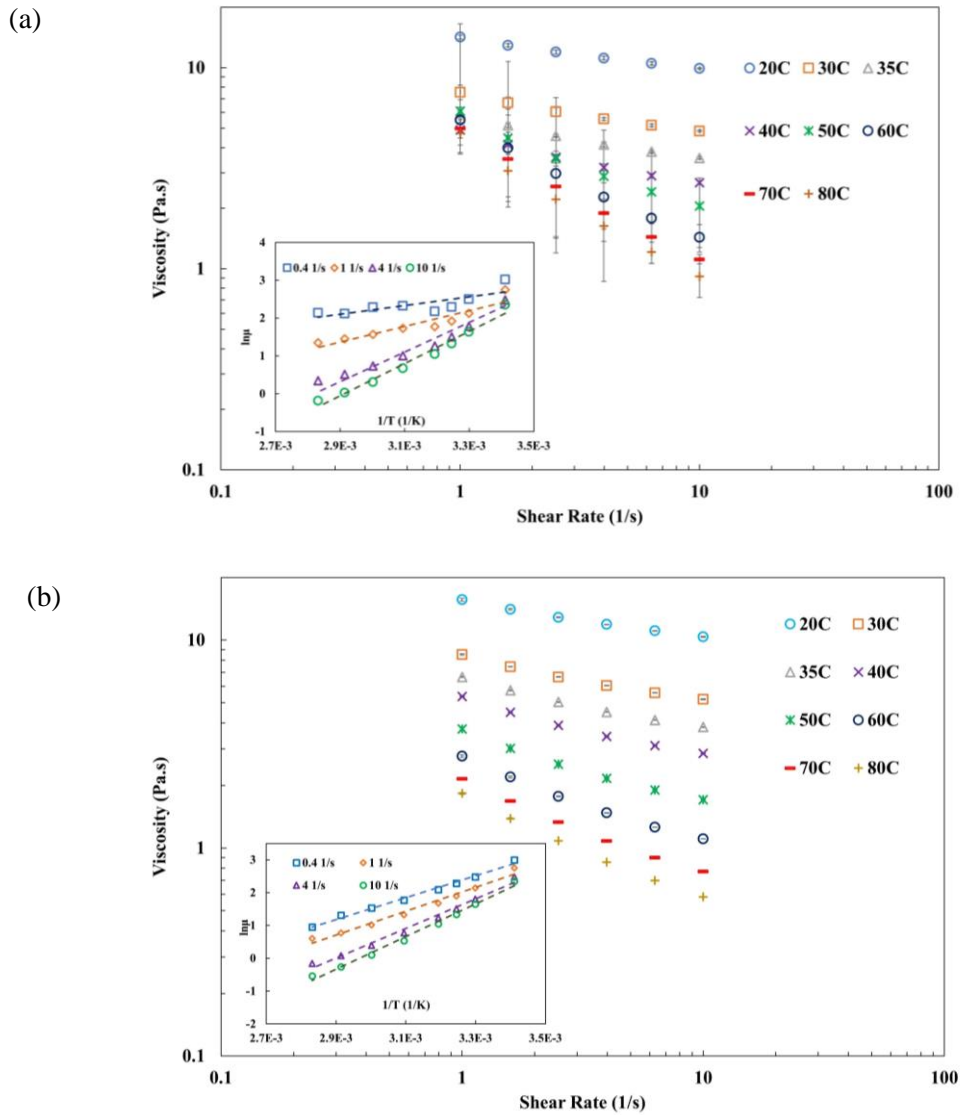


Figure 4.4 Viscosity of nanofluids in ETC at isothermal conditions across tested shear rates 1 s^{-1} to 10 s^{-1} (Inset) $\ln \eta$ vs. $1/T$ at tested shear rates (a) N0.5 (b) N1

4.4.2 Analytical model – viscosity vs. temperature gradient

The isothermal viscosity data was plotted in the form of $\ln \eta$ vs. $1/T$ (Figure 4.4a and 4.4b inset) to obtain the fit parameters A and B according to Equation 11. Unlike glycerol, the fit parameters are shear-rate dependent as seen in Figure 4.5.

Similar to the analytical model that could determine the viscosity of glycerol, the energy equation and viscosity-temperature relationship was coupled and solved for viscosity.

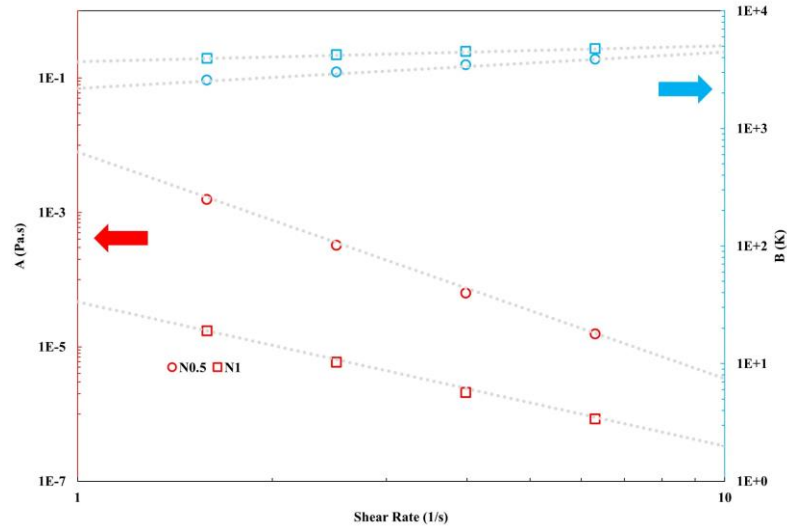


Figure 4.5 Fit parameters of N0.5 and N1 at tested shear rates (a) A (primary y axis) (b) B (secondary y axis); both parameters A and B exhibit shear rate dependence which is fit to a power curve

The shear thinning behaviour of the nanofluid which is observed under isothermal conditions is still visible under a temperature gradient as seen in Figure 4.6.

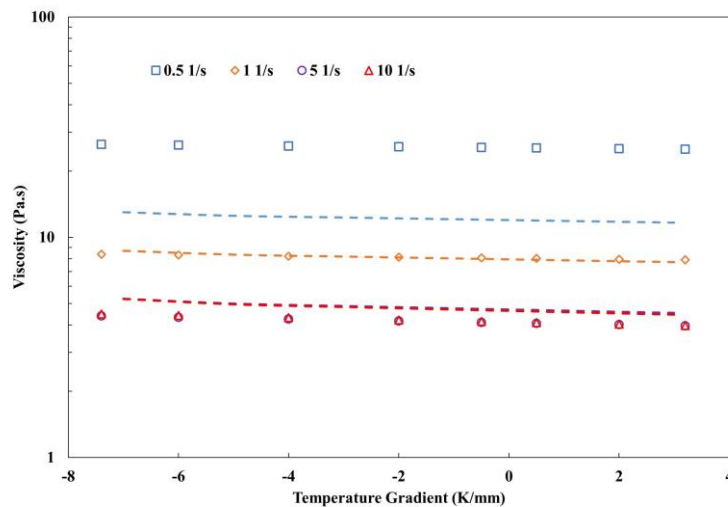


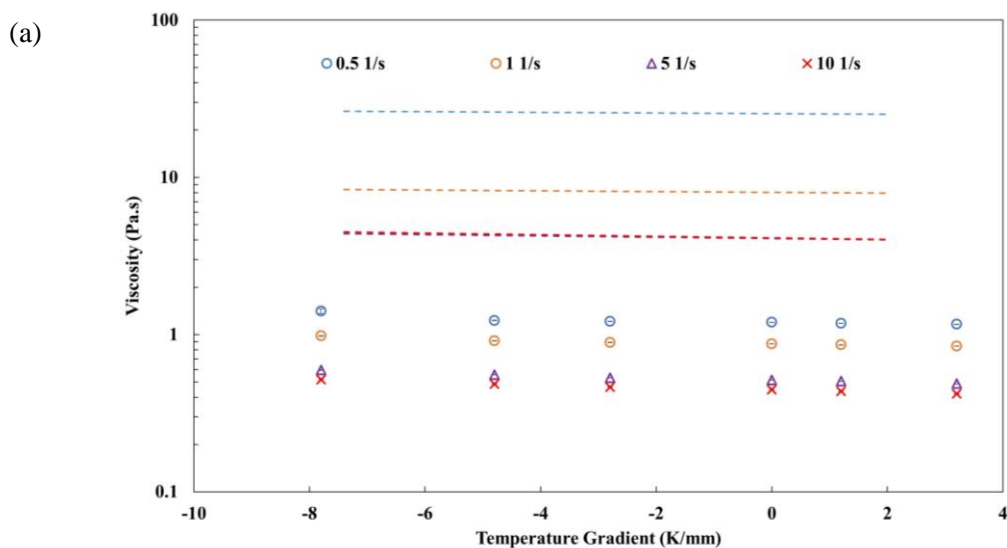
Figure 4.6 Model viscosity vs. temperature gradient of N0.5 (discrete points) and N1 (dashed line)

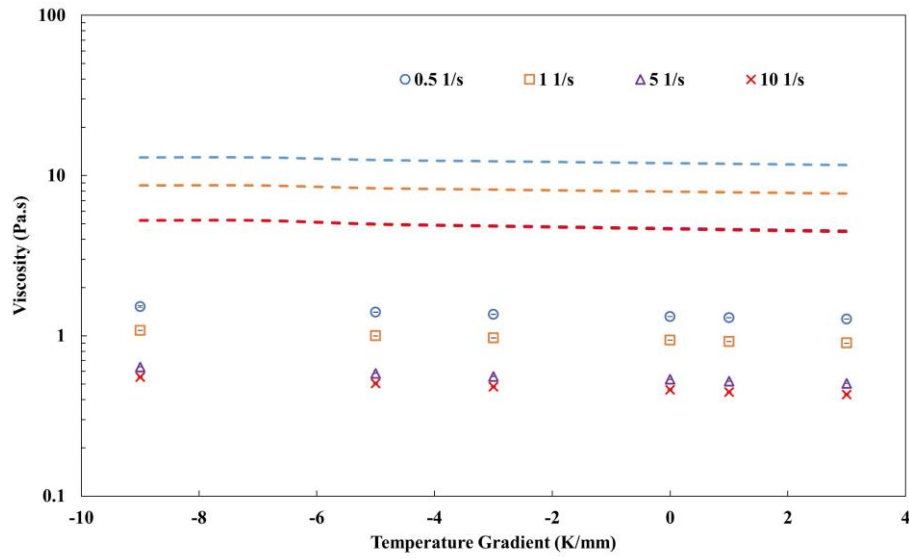
On comparing N0.5 and N1, the viscosity under temperature gradient is equal for both the weight fractions except at 0.5 s^{-1} where N0.5 exhibits an inflated viscosity. This may be attributed to inertial effects in the isothermal experiment which has caused an increase in the fit parameters leading to an inflated viscosity of N0.5.

4.4.3 Experimental – viscosity vs temperature gradient

N0.5 and N1 were also tested in the heat flux apparatus to study the coupled dynamics of fluid flow and heat flow in non-Newtonian fluids. Similar to the analytical model, an increase in temperature gradient leads to a fall in viscosity (Figure 4.7). The shear thinning behaviour of the nanofluid under isothermal conditions which is captured by the analytical model can also be observed in the experimental rheological data.

Although the trend of viscosity with shear rate and temperature gradient is similar for both the model and the experimental counterpart, the model overestimates the viscosity of the nanofluid across the tested temperature gradients for both N0.5 and N1 (Figure 4.7). This overestimation is similar to the model vs. experimental data for glycerol (Figure 3.4).





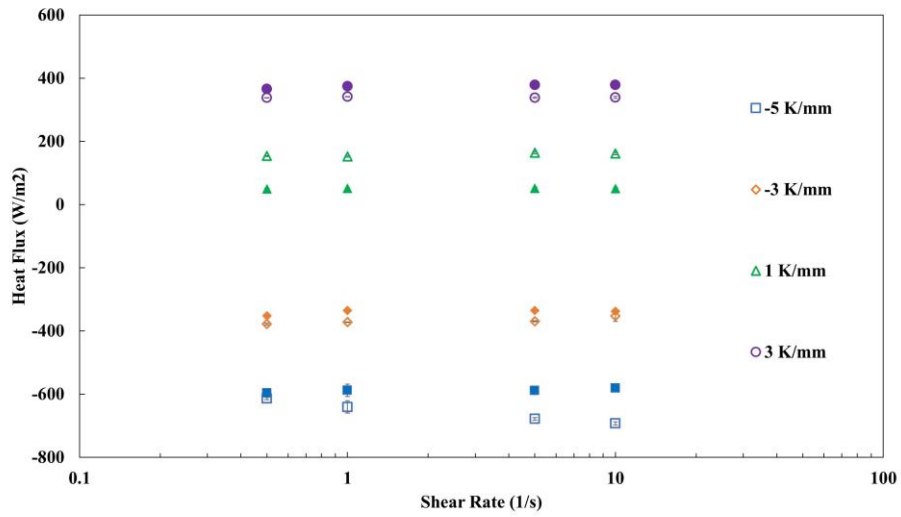
(b)

Figure 4.7 Viscosity vs. temperature gradient – analytical model (dashed lines) and experimental (discrete points) values (a) N0.5 (b) N1

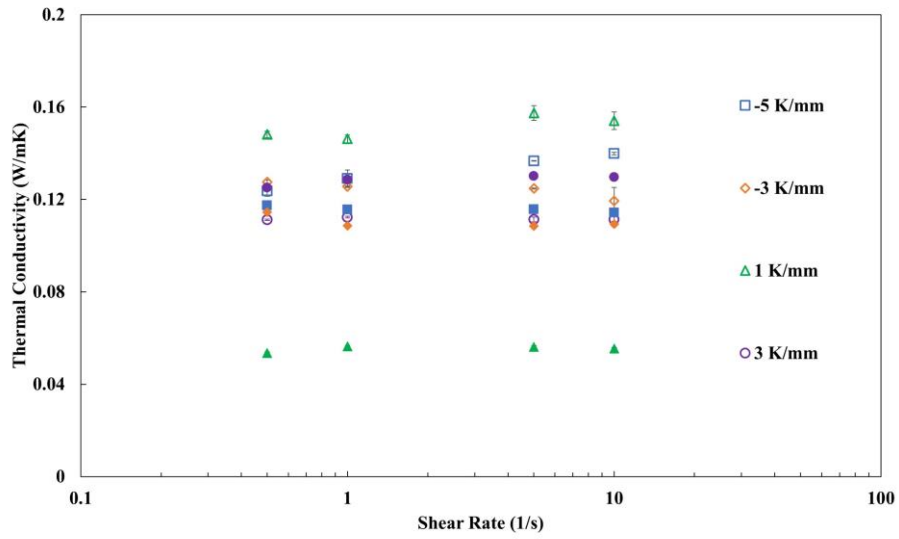
The difference in the measured viscosity in the ETC oven and heat flux apparatus translates into a gap between the model and experiment as the model fit parameters are obtained by the viscosity-temperature trends in the ETC. A deeper investigation into the measurement techniques differences between the ETC and Heat Flux apparatus will lead to explaining the gap between the model and experiment, and subsequently attempt to bridge it.

4.5 Thermal Properties of Nanofluid

The heat flux of the nanofluid was measured and corrected for the air gap and the thermal conductivity of the nanofluid was also calculated. On comparison between the thermal conductivities of pure glycerol and CNT nanofluids, it is observed that the increase in thermal conductivity is negligible on addition of the CNT particles. Similar to glycerol base fluid, the thermal conductivity and heat flux of the nanofluid does not change with shear rate within the range of tested shear rates as seen in Figure 4.8.



(a)



(b)

Figure 4.8 Experimental values at $T_{LHP} 35^{\circ}\text{C}$ (a) Thermal conductivity vs. shear rate (b) Heat flux vs. shear rate; N0.5 (Hollow points) and N1 (Filled points)

4.6 Scaling of coupled dynamics

Similar to glycerol, the coupled dynamics of heat and fluid flow in N0.5 and N1 was scaled using two dimensionless quantities – Br and Ri . As seen in Figure 4.9, the experimental data at $T_{LHP} 35^{\circ}\text{C}$ of both N0.5 and N1 collapsed on a single curve except at very low Ri *i.e.* $Ri < 10^{-4}$.

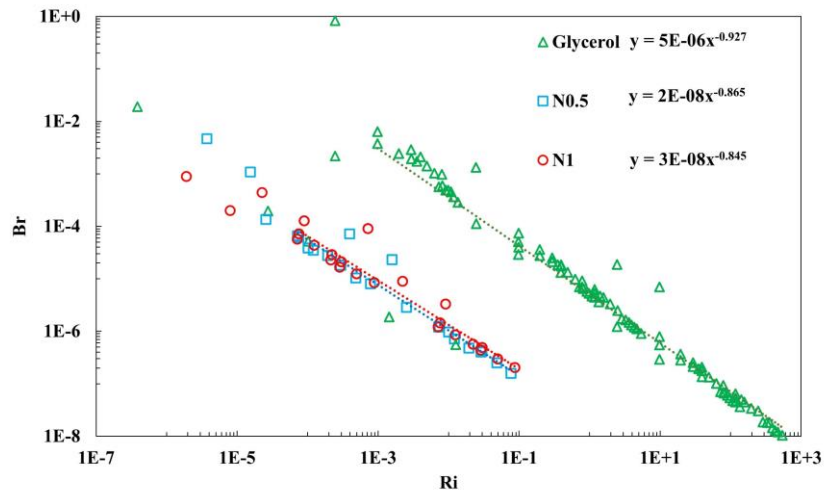


Figure 4.9 Scaled transport dynamics of coupled heat and fluid flow of N0.5 and N1 at T_{LHP} : 35°C – Br. vs. Ri

The value of the fit parameters for both N0.5 and N1 according to Equation 19 is $\delta \sim 3 \times 10^{-8}$ and $\varepsilon \sim -0.85$. Thus, in comparison to glycerol, the value of ε is lower, although data at other T_{LHP} will help in obtaining a better fit. In comparison with glycerol, the value of δ has reduced on addition of CNT. Thus, at equal values of Ri, the nanofluid would yield a lower Br which is due to a higher heat flux through the sample.

CHAPTER V

CONCLUSION AND FUTURE RESEARCH

5.1 Conclusion

The coupled dynamics of fluid flow and heat flow are explored in this thesis.

The design of a rheometric accessory that enables the orthogonal superimposition of temperature gradient with shear deformation is presented. A parallel plate accessory is chosen to enable a uniform temperature gradient across the fluid sample. It is possible to measure the rheological and thermal properties with the help of this accessory.

The device and technique were validated using glycerol which is a Newtonian fluid. The viscosity of glycerol under an imposed temperature gradient was analytically modelled and compared with the experimentally obtained values. It was observed that both the data sets exhibited a decrease in viscosity with increase in temperature gradient. Although the model overestimates the value of the viscosity, they are within the same order.

The thermal conductivity and heat flux values were numerically calculated and compared to the experimental values. An engineering oversight in the test plate led to an air gap in the LHP which increased the thermal resistance of the system. Thus, the experimental values of heat flux were

corrected for the air gap and the corrected values were calculated. The experimental values are lower than the numerically calculated values and this gap can be understood and bridged by further perfecting the protocol for the presence of the air gap. Even though the magnitude of the thermal properties is lower than the numerically calculated ones, both the data sets exhibit a similar trend; neither thermal conductivity nor heat flux is affected by shear rate.

The apparatus is validated by investigating the relationship of the Brinkman Number with shear rate and temperature gradient. The experimental data is scaled with Brinkman number and Richardson number which implied that Br is inversely proportional to Ri and an increase in Ri leads to lesser entropy production in the system.

Similar experiment and analyses were performed on nanofluids of CNT in glycerol at two weight fractions. The nanofluid was shear thinning and the viscosity of the nanofluid with temperature gradient was analytically modelled and compared to the experimental values. The trend of both the model and experimental results agree with each other, although the model overestimates the viscosity. The viscosities of both the weight fractions do not show appreciable difference between them.

The heat flux and thermal conductivities were measured and corrected for the air gap. It was observed that the heat flux and thermal conductivities of the nanofluids are not affected shear rate in the range of shear rates tested. The experimental data was scaled with the Brinkman number and Richardson number; the data sets for both the suspensions collapse on a single curve at the higher Ri range. At the lower ranges, there is scatter in the data set.

5.2 Future Research

5.2.1 Design Improvements

Similar to an in-house LHP, a novel UHP can be designed and fabricated. Since the current UHP (procured from TA) can achieve a maximum of 100°C, an in-house UHP can help overcome this particular barrier and help achieve far-from-equilibrium conditions which may yield interesting transport dynamics. The challenge in designing a UHP stems from the requirement of heating and measuring the temperature of the plate without contact. This can be overcome with the help of convective heating via band heater and a heat spreader whereas non-contact IR thermocouples can aid in temperature measurement.

The correction of heat flux reported by the sensor due to the air gap can be analysed further to bridge the gap between numerically calculated thermal conductivity values and that reported by the sensor. A separate LHP test plate can be redesigned and fabricated to overcome the engineering oversight that induced an air gap in the thermal circuit.

The range of shear rates tested can be widened to investigate the effect of high shear and very low shear on the heat transfer properties.

5.2.2 Test Material Selection

The coupled dynamics of heat and fluid flow can be studied for a variety of materials that extend into rheologically diverse fluids such as shear-thinning, shear thickening and also includes the time dependent fluid flow regimes such as thixotropy and rheopexy. Different class of materials based on composition can also be studied such as monolithic fluids, colloids, suspensions, gels etc. A phase diagram of CNT in glycerol can be constructed with respect to the coupled dynamics of heat and fluid flow.

The effect of gravity on the coupled dynamics of both the transport processes can be studied by the Heat Flux Apparatus since gradients in both directions i.e. co and counter gravity can be established.

REFERENCES

- ¹ Richard S. Lindzen and Sumant Nigam. 1987. On the role of sea surface temperature gradients in forcing low-level winds and convergence in the tropics. *Journal of the Atmospheric Sciences* 44, 17, 2418–2436.
- ² Anat Bahat, S. R. Caplan, and Michael Eisenbach. 2012. Thermotaxis of human sperm cells in extraordinarily shallow temperature gradients over a wide range. *PLoS one* 7, 7.
- ³ Horst H. Winter. 1977. Viscous dissipation in shear flows of molten polymers. *Advanced Heat Transfer* 13, 205–267.
- ⁴ Yunus A. Cengel. 2003. *Heat and Mass Transfer: A Practical Approach*. McGraw Hill Education, Columbus, GA, USA.
- ⁵ Carl L. Yaws and Chaitanya Gabbula. 2003. *Handbook of Thermodynamic and Physical Properties of Chemical Compounds*. Knovel.
- ⁶ Christopher W. Macosko and Ronald G. Larson. 1994. *Rheology: principles, measurements and applications*. John Wiley & Sons,
- ⁷ Naveed Ahmad. 2013. *Relationship between Rheology and Molecular Structure of Innovative Crystalline Elastomers* (2013). Retrieved from.
- ⁸ Vinod Yadav, Vijay K. Jain, and Prakash M. Dixit. 2002. Thermal stresses due to electrical discharge machining. *International Journal of Machine Tools and Manufacture* 42, 8, 877–888.

- ⁹ Subrahmanyam Chandrasekhar. 2013. *Hydrodynamic and hydromagnetic stability*. Courier Corporation.
- ¹⁰ Daniele Vigolo, Roberto Rusconi, Howard A. Stone, and Roberto Piazza. 2010. Thermophoresis: microfluidics characterization and separation. *Soft Matter* 6, 15, 3489–3493.
- ¹¹ G. Pitarresi and E. A. Patterson. 2003. A review of the general theory of thermoelastic stress analysis. *The Journal of Strain Analysis for Engineering Design* 38, 5, 405–417.
- ¹² Klaus Clusius. 1938. Neues verfahren zur gasentmischung und isotopentrennung. *Natur-wiss* 33, 546.
- ¹³ Simone Wiegand. 2015. *Introduction to thermal gradient related effects* (2015). Retrieved from.
- ¹⁴ Ping Sheng and Weijia Wen. 2012. Electrorheological fluids: mechanisms, dynamics, and microfluidics applications. *Annual review of fluid mechanics* 44, 143–174.
- ¹⁵ Bong J. Park, Fei F. Fang, and Hyoung J. Choi. 2010. Magnetorheology: materials and application. *Soft Matter* 6, 21, 5246–5253.
- ¹⁶ P. D. Shima, John Philip, and Baldev Raj. 2009. Magnetically controllable nanofluid with tunable thermal conductivity and viscosity. *Applied physics letters* 95, 13, 133112.
- ¹⁷ James W. Goodwin, Gavin M. Markham, and Brian Vincent. 1997. Studies on model electrorheological fluids. *The Journal of Physical Chemistry B* 101, 11, 1961–1967.

- 18 William. B. Krantz. 2007. *Scaling Analysis in Modelling Transport and Recation Processes: A systematic approach to model building and the art of approximation*. John Wiley & Sons,
- 19 J. A. Falade, S. O. Adesanya, J. C. Ukaegbu, and M. O. Osinowo. 2016. Entropy generation analysis for variable viscous couple stress fluid flow through a channel with non-uniform wall temperature. *Alexandria Engineering Journal* 55, 1, 69–75.
- 20 L. V. McIntire and W. R. Schowalter. 1970. Stability of viscoelastic fluids: Couette flow with superposed temperature gradient. *Transactions of the society of rheology* 14, 4, 585–603.
- 21 Hamdy Hassan, Nicolas Regnier, Cyril Pujos, and Guy Defaye. 2008. Effect of viscous dissipation on the temperature of the polymer during injection molding filling. *Polymer Engineering and Science* 48, 6, 1199–1206.
- 22 Simone Wiegand. 2004. Thermal diffusion in liquid mixtures and polymer solutions. *Journal of Physics: Condensed Matter* 16, R357-R379.
- 23 Richard J. Goldstein, H. D. Chiang, and D. L. See. 199. High-Rayleigh-number convection in a horizontal enclosure. *Journal of Fluid Mechanics* 213 (199), 111–126.
- 24 Henri Benard. 1901. Les tourbillons cellulaires dans une nappe liquide propageant de la chaleur par convection: en régime permanent. *Journal of Physics: Theories and Applications* 10, 1, 254–266.
- 25 Lord Rayleigh. 1916. On convective currents in a horizontal layer of fluid when the higher temperature is on the under side. *Philisophical Magazine* 32, 529–546.

- ²⁶ M. Lamsaadi, M. Naimi, and M. Hasnaoui. 2005. Natural convection of non-Newtonian power law fluids in a shallow horizontal rectangular cavity uniformly heated from below. *Heat and Mass Transfer* 41, 3, 239–249.
- ²⁷ Zineddine Kebiche, Cathy Castelain, and Teodor Burghelea. 2014. Experimental investigation of the Rayleigh-Benard convection in a yield stress fluid. *Journal of Non-Newtonian Fluid Mechanics* 203, 9–23.
- ²⁸ Lubomira Broniarz-Press and Karol Pralat. 2009. Thermal conductivity of Newtonian and non-Newtonian liquids. *International Journal of Heat and Mass Transfer* 52, 21-22, 4701–4710.
- ²⁹ Chih P. Tso, C. H. Hor, G. M. Chen, and C. K. Kok. 2018. Heat induction by viscous dissipation subjected to symmetric and asymmetric boundary conditions on a small oscillating flow in a microchannel. *Symmetry* 10, 10, 499.
- ³⁰ Mourad Kaddiri, Mohamed Naimi, Abdelghani Raji, and Mohammed Hasnaoui. 2012. Rayleigh-Benard convection of non-Newtonian Power-law fluids with temperature-dependent viscosity. *ISRN Thermodynamics* 2012.
- ³¹ Z. Alloui and P. Vasseur. 2015. Natural convection of Carreau-Yasuda non-Newtonian fluids in a vertical cavity heated from the sides. *International Journal of Heat and Mass Transfer* 84, 912–924.
- ³² Osman Turan, Nilanjan Chakraborty, and Robert J. Poole. 2010. Laminar natural convection of Bingham fluids in a square enclosure with differentially heated side walls. *Journal of Non-Newtonian Fluid Mechanics* 165, 15-16, 901–913.
- ³³ Yanchao Yin, Liran Ma, Xuefung Xu, Yu Tian, Shizhu Wen, and Jianbin Luo. 2019. Thinning of glycerol in the presence of multi-walled carbon nanotubes. *The Journal of Chemical Physics* 151, 54302.

- ³⁴ John B. Segur and Helen E. Oberstar. 1951. Viscosity of glycerol and its aqueous solutions. *Industrial & Engineering Chemistry* 43, 9, 2117–2120.
- ³⁵ Yen M. Chen and Arne J. Pearlstein. 1987. Viscosity-temperature correlation for glycerol-water solutions. *Industrial & Engineering Chemistry research* 26, 8, 1670–1672.
- ³⁶ Oscar K. Bates. 1936. Binary mixtures of water and glycerol-thermal conductivity of liquids. *Industrial & Engineering Chemistry* 28, 4, 494–498.
- ³⁷ C. Talon, Q. W. Zou, Ramos MA, R. Villar, and S. Vieira. 2001. Low-temperature specific heat and thermal conductivity of glycerol. *Physical Review B* 65, 1, 12203.
- ³⁸ E. D.C. Andrade. 1934. LVIII A theory of the viscosity of liquids - Part II. *The London, Edinburgh, and Dublin Philosophical Magazine and Journal of Science* 17, 113, 698–732.
- ³⁹ Clovis R. Maliska. 1990. On the physical significance of some dimensionless numbers used in heat transfer and fluid flow. *Federal University of Santa Catarina, Florianopolis, SC*.
- ⁴⁰ Ved P. Sharma, Utkarsh Sharma, Mahadev Chattopadhyay, and V. N. Shukla. 2018. Advance Applications of Nanomaterials: A Review. *Materials Today: Proceedings* 5, 2, 6376–6380.
- ⁴¹ Roozbeh Rafati, Sean R. Smoth, Amin S. Haddad, Rizky Novara, and Hossein Hamidi. 2018. Effect of nanoparticles on the modifications of drilling fluids properties: A review of recent advances. *Journal of Petroleum Science and Engineering* 161, 61–76.
- ⁴² Rahman Saidur, S. N. Kazi, M. M. Hossain, and H. A. Mohammed. 2011. A review on the performance of nanoparticles suspended with refrigerants and

- lubricating oils in refrigeration systems. *Renewable and Sustainable Energy Reviews* 15, 1, 310–323.
- 43 H. J. Lee, S. H. Lee, Choi C, S. Jang, and S. Choi. 2011. A review of thermal conductivity data, mechanisms and models for nanofluids. *International journal of micro-nano scale transport* 1, 4, 269–322.
- 44 Xiang-Qi Wang and Arun S. Mujumdar. 2007. Heat transfer characteristics of nanofluids: a review. *International Journal of Thermal Sciences* 46, 1, 1–19.
- 45 Sezer Ozerinc, Sadik Kakac, and Almila G. Yazicioglu. 2010. Enhanced thermal conductivity of nanofluids: a state-of-the-art review. *Microfluidics and Nanofluidics* 8, 2, 145–170.
- 46 Stephen U. Choi. 2009. Nanofluids: from vision to reality through research. *Journal of Heat Transfer* 131, 3.
- 47 S. Halelfadl, P. Estellé, B. Aladag, N. Doner, and T. Maré. 2013. Viscosity of carbon nanotubes water-based nanofluids: Influence of concentration and temperature. *International Journal of Thermal Sciences* 71, 111–117.
- 48 Prabhat Agnihotri, Sumit Basu, and K. K. Kar. 2011. Effect of carbon nanotube length and density on the properties of carbon nanotube-coated carbon fiber/polyester composites. *Carbon* 49, 9, 3098–3106.
- 49 Peter Burke, Zhengyu Yu, S. Li, and Chris Rutherglen. 2005. *Nanotube technology for microwave applications*, 2005.
- 50 Yoshikazu Homma, Satoru Suzuki, Yoshihiro Kobayashi, Masao Nagase, and Daisuke Takagi. 2004. Mechanism of bright selective imaging of single-walled carbon nanotubes on insulators by scanning electron microscopy. *Applied physics letters* 84, 10, 1750–1752. DOI: <https://doi.org/10.1063/1.1667608>.

- ⁵¹ Rad Sadri, Goodarz Ahmadi, Hussein Togun, Mahidzal Dahari, Salim N. Kazi, Emad Sadeghinezhad, and Nashrul Zubir. 2014. An experimental study on thermal conductivity and viscosity of nanofluids containing carbon nanotubes. *Nanoscale research letters* 9, 1, 151.
- ⁵² H. A. Mohammed, A. A. Al-Aswadi, N. H. Shuain, and R. Saidur. 2011. Convective heat transfer and fluid flow study over a step using nanofluids: a review. *Renewable and Sustainable Energy Reviews* 15, 6, 2921–2939.
- ⁵³ Abdelhafid Abouharim, Abdelghafour Moutarajji, and Khalil El-Hami. 2019. Effect of Multiwall Carbon Nanotube Concentration on Thermal and Electrical Properties of Glycerol Nanofluid International Conference on Advanced Intelligent Systems for Sustainable Development, 297–305.
- ⁵⁴ S. M.S. Murshed, K. C. Leong, and C. Yang. 2008. Investigations of thermal conductivity and viscosity of nanofluids. *International Journal of Thermal Sciences* 47, 5, 560–568.
- ⁵⁵ L. A. Bulavin, N. I. Lebovka, Y. A. Kyslyi, S. V. Chrapatyi, A. I. Goncharuk, I. A. Mel'nyk, and V. I. Koval'chuk. 2011. Microstructural, rheological, and conducto-metric studies of multiwalled carbon nanotube suspensions in glycerol. *Ukrainian Journal of Physics* 56, 3, 217.
- ⁵⁶ Thathan Premkumar, Raffaele Mezzenga, and Kurt E. Geckeler. 2012. Carbon nanotubes in the liquid phase: addressing the issue of dispersion. *Small* 8, 9, 1299–1313.
- ⁵⁷ Wei Yu and Huaqing Xie. 2012. A review on nanofluids: preparation, stability mechanisms, and applications. *Journal of nanomaterials*.

- ⁵⁸ Ying Yang, E. A. Grulke, George Z. Zhang, and Gefei Wu. 2006. Thermal and rheological properties of carbon nanotube-in-oil dispersions. *Journal of Applied Physics* 99, 11, 114307.